1   **Dissecting the collateral damage of antibiotics on gut microbes**

2   Lisa Maier[1,7#*], Camille V. Goemans[1#], Mihaela Pruteanu[1,8], Jakob Wirbel[2], Michael Kuhn[2,]

3   Elisabetta Cacace[1], Tisya Banerjee[1], Exene Erin Anderson[1,9], Alessio Milanese[2], Ulrike

4   Löber[3,4], Sofia K. Forslund[2,3,4], Kiran Raosaheb Patil[2], Georg Zeller[2], Peer Bork[2,4,5,6] and

5   Athanasios Typas[1,2*]

6

7   # These authors contributed equally to this work

8   * Correspondence: typas@embl.de and l.maier@uni-tuebingen.de

9
10   [1]European Molecular Biology Laboratory, Genome Biology Unit, Heidelberg, Germany

11   [2]European Molecular Biology Laboratory, Structural and Computational Biology Unit,

12   Heidelberg, Germany

13   [3] Experimental and Clinical Research Center, a cooperation of Charité - Universitätsmedizin

14   Berlin and Max Delbruck Center for Molecular Medicine, Berlin, Germany

15   [4] Max-Delbrück-Center for Molecular Medicine, Berlin, Germany

16   [5] Molecular Medicine Partnership Unit, Heidelberg, Germany

17   [6] Department of Bioinformatics, Biocenter, University of Würzburg, Germany

18   [7] current address: Interfaculty Institute of Microbiology & Infection Medicine Tübingen,

19   Germany

20   [8] current address: Institute for Biology, Humboldt University Berlin, Germany

21   [9] current address: NYU School of Medicine, New York, USA

22

23

Abstract

Antibiotics are used for fighting pathogens, but also target our commensal bacteria as a side effect, disturbing the gut microbiota composition and causing dysbiosis and disease[1-3]. Despite this well-known collateral damage, the activity spectrum of the different antibiotic classes on gut bacteria remains poorly characterized. Having monitored the activities of >1,000 marketed drugs on 38 representative species of the healthy human gut microbiome[4], we here characterize further the 144 antibiotics therein, representing all major classes. We determined >800 Minimal Inhibitory Concentrations (MICs) and extended the antibiotic profiling to 10 additional species to validate these results and link to available data on antibiotic breakpoints for gut microbes. Antibiotic classes exhibited distinct inhibition spectra, including generation-dependent effects by quinolones and phylogeny-independence by β-lactams. Macrolides and tetracyclines, two prototypic classes of bacteriostatic protein synthesis inhibitors, inhibited almost all commensals tested. We established that both kill different subsets of prevalent commensal bacteria, and cause cell lysis in specific cases. This species-specific activity challenges the long-standing divide of antibiotics into bactericidal and bacteriostatic, and provides a possible explanation for the strong impact of macrolides on the gut microbiota composition in animals[5-8] and humans[9-11]. To mitigate the collateral damage of macrolides and tetracyclines on gut commensals, we exploited the fact that drug combinations have species-specific outcomes in bacteria[12] and sought marketed drugs, which could antagonize the activity of these antibiotics in abundant gut commensal species. By screening >1,000 drugs, we identified several such antidotes capable of protecting gut species from these antibiotics without compromising their activity against relevant pathogens. Altogether, this study broadens our understanding of antibiotic action on gut commensals, uncovers a previously unappreciated and broad bactericidal effect of prototypical bacteriostatic antibiotics on gut bacteria, and opens avenues for preventing the collateral damage caused by antibiotics on human gut commensals.

50 **MAIN TEXT**

51 Medication is emerging as major contributor for changes in the composition of the human gut

52 microbiota[4,13-15]. Such severe and long-lasting changes are associated, and in some cases

53 causatively linked, to dysbiosis and a wide range of diseases[16]. Although several non-

54 antibiotic drugs may also have a previously unappreciated impact on the gut microbiome

55 composition[4,16,17], antibiotics, developed to have broad spectra and thereby target very

56 diverse pathogens, are long known to take a heavy toll on our gut flora, causing a variety of

57 gastrointestinal side-effects[18], including *Clostridioides (former Clostridium) difficile* infections.

58 Recently more attention has been given to this collateral damage of antibiotics on the gut

59 microbiota and thereby on the host's wellbeing. *In vivo* studies highlight links between the

60 long-term microbiota compositional changes and host dysbiosis, including the development

61 of allergic, metabolic, immunological and inflammatory diseases[5-8,10,11,19-21]. While uncovering

62 the direct effects of different antibiotics on our gut flora is critical to improve general health,

63 technical difficulties hamper routine testing of antibiotic susceptibility in anaerobes[22,23].

64 Currently available data on bacterial susceptibility to antibiotics is focused on invasive

65 pathogens and offers little to no resolution in the diversity of the human gut microbiota[24].

66 Information is missing even for the most prevalent and abundant gut species, or ones

67 recently associated with dysbiosis and disease[25,26]. In addition, existing animal or cohort

68 studies have used a handful of antibiotics or merge data from different antibiotic classes,

69 precluding systematic and general conclusions on the matter.

70 We recently assessed the direct effect of ~1200 FDA-approved drugs on the growth

71 of 38 prevalent and abundant or disease-associated human gut species under anaerobic

72 conditions at a fixed concentration of 20 μM[4]. This initial screen (referred to hereafter as

73 "screen") included 144 antibiotics (Fig. 1a, Extended Data Fig. 1, Suppl. Table 1), with

74 different classes having discernible effects on gut microbes (Fig. 1b). We validated these

75 results by measuring 815 MICs (33 antibiotics and 2 antifungals for 17 species, 22 antibiotics

76 for 10 additional species), using MIC gradient test strips (Fig. 1a, Extended Data Fig. 2,

77 Suppl. Table 2 + 3). Despite differences in the experimental procedure, concordance

3

78   between data from the initial screen and MICs is very high: Specificity and sensitivity of 0.97

79   (Extended Data Fig. 3a). The newly established MICs also correlate well with available data

80   on antimicrobial susceptibility from databases such as EUCAST[24] or ChEMBL[27] (r_s=0.69 and

81   r_s=0.64, respectively), despite differences in strains and media used (Extended Data Fig. 3b).

82   Importantly, this new dataset considerably expands the available MICs, as much as by 80%

83   for non-pathogenic bacteria (Fig. 1c, Extended Data Fig. 3c). Altogether, the initial screen

84   and the new MIC dataset provide high-resolution information on the target spectrum of

85   antibiotics on commensal gut microbes, which we explored further.

86   The antibiotics tested exhibited strong class-dependent effects (Fig. 1b, d).

87   Consistent with literature, aminoglycosides hardly affected gut microbes under anaerobic

88   conditions[28] and sulfonamides were inactive in the medium used for the screen[4]. Quinolones

89   acted in a generation-dependent manner. First-generation variants were effective only on a

90   narrow spectrum of microbes that included both commensal *E. coli* tested. Second- and

91   third- generation quinolones increased the spectrum. Fourth-generation variants (developed

92   to increase activity against anaerobes) inhibited all tested species, except for *Akkermansia*

93   *muciniphila* (Fig. 1e, Extended Data Fig. 1, red box), a species associated with protection

94   against different diseases and dysbiotic states[29], and even positive responses to

95   immunotherapy[30]. For β-lactams, resistance was patchy but distinct for different members

96   and subclasses (Extended Data Fig. 2, 4a). For *Bacteroidetes*, we tested additional species

97   and strains (in total 12 and 19, respectively) (Extended Data Fig. 4b, c), confirming that β-

98   lactam sensitivity and phylogenetic relatedness are uncoupled (Extended Data Fig. 4d). This

99   argues for resistance mechanisms being strain-specific and horizontally transferred.

100   Macrolides showed a strong impact on gut commensals and inhibited all tested microbes

101   (Fig. 1d), except for the opportunistic pathogen *C. difficile*, which was resistant to all tested

102   macrolides and clindamycin (Extended data Fig. 2, red box). This is in line with the

103   associated risk of *C. difficile* infection after macrolide/clindamycin treatment[31]. Finally, 8 of

104   the 9 tested tetracyclines inhibited nearly all tested microbes, which is surprising in the light

105   of the gut microbiota being considered as reservoir for tetracycline resistance genes[32].

4

106   Concentration-resolved MICs confirmed the same drug class-dependent trends observed in

107   the screen (Fig. 1d, f). In addition, MICs allow for comparisons with clinical breakpoints, i.e.

108   MICs at which a species should be considered resistant or susceptible (Fig. 1f). Overall, the

109   gut microbes in our assays (anaerobic growth, gut mimetic growth medium[33]) were slightly

110   more resistant to most antibiotic classes than previously reported for pathogens (aerobic

111   growth, Mueller-Hinton agar). Tetracyclines were the exception, inhibiting commensals at

112   significantly lower concentrations than what is reported for pathogens (Fig. 1f). Thus,

113   commensals might be considerably less resistant to tetracyclines than previously anticipated

114   and suggested by the detection of tetracycline resistance elements in fecal metagenomes.

115   Recent *in-vivo* studies have shown that β-lactams and macrolides have a strong and

116   long-lasting collateral impact on the gut microbiota composition and thereby on host health[5-8].

117   As β-lactams exhibited strain-specific effects (Extended Data Fig. 1, 2, 4) and are known to

118   kill bacteria (bactericidal), they could *irrevocably* deplete *specific* members of the gut

119   microbiota, thereby explaining their differential and long-lasting effects on the community

120   composition. On the other hand, macrolides uniformly targeted all tested gut commensals

121   (Fig. 1d) and are textbook bacteriostatic antibiotics, i.e. inhibit bacterial growth, but do not kill

122   (at least at high numbers). In this case, the long-term community composition change is

123   more difficult to rationalize, as all community members are inhibited, but should be able to

124   regrow once drug is removed. Similarly, tetracyclines, another class of bacteriostatic

125   antibiotics that acted on nearly all gut microbes we tested, have known gastro-intestinal side-

126   effects[18], which are indicative of gut microbiome dysbiosis. We thus wondered at which level

127   macrolides and tetracyclines exert a differential effect on gut microbes. Although traditionally

128   both clinical use[34-37] and basic research[38,39] heavily rely on this distinction between

129   bactericidal and bacteriostatic antibiotics, there are reports of drugs changing their killing

130   capacity depending on the organism, drug concentration or medium tested[40,41] (and

131   increased evidence from meta-analyses that the distinction may have little relevance to

132   clinical practice[42,43]). We therefore hypothesized that this bacteriostatic/bactericidal divide

133   may be less rigid for gut commensals, which are more phylogenetically diverse than the few

134   pathogens usually tested, and hence provide a level where the effect of these drug classes

135   on gut microbes becomes differential.

136   The standard way to determine whether an antibiotic has bactericidal or bacteriostatic

137   activity is to calculate time-kill curves, where the bacterial survivors are counted on agar at

138   various time-points after drug treatment. If, over a significant period of antibiotic treatment

139   (ranging from 5 to 24 hours), the number of colony forming units (CFU)/ml of culture

140   decreases by more than 99.9%, the antibiotic is considered bactericidal[40]. We assessed the

141   survival of 12 abundant gut microbes over a 5-hour treatment of either a macrolide

142   (erythromycin or azithromycin) or a tetracycline (doxycycline) at 5 x MIC (Fig 2a + b,

143   Extended Data Fig. 5). About half of the tested species decreased in survival by >99.9%,

144   pointing to these drugs being bactericidal to several abundant gut microbes. To confirm this

145   further, we tested the viability of *B. vulgatus* and *E. coli* ED1a upon erythromycin,

146   azithromycin or doxycycline treatments using live/dead staining. Microscopy and flow

147   cytometry assessment of live/dead bacteria corroborated the initial observations (Fig. 2c,

148   Extended Data Fig. 6). As tetracyclines are considered bona-fide bacteriostatic drugs in *E.*

149   *coli*, we were surprised to see that doxycycline effectively killed the commensal *E. coli* ED1a

150   (Fig. 2a). We verified that these effects held also in the presence of oxygen (Extended Data

151   Fig. 7a) and confirmed that doxycycline has a stronger bactericidal action on this natural

152   isolate than on the domesticated *E. coli* K-12 lab strain, BW25113 (Extended Data Fig. 7b).

153   In parallel, we excluded that the differences in killing capacity were confounded by growth

154   rate, growth phase or MIC of the bacterial species tested (Extended Data Fig. 8). We also

155   noticed that *B. vulgatus* and *B. uniformis* cultures decreased density in the presence of

156   erythromycin (Fig. 2d). We confirmed by time-lapse microscopy that this was due to lysis.

157   Erythromycin caused cell shape defects, including blebbing, cytoplasmic shrinkage, and

158   ultimately cell lysis in both *B. vulgatus* and *B. uniformis* (Figure 2e, Movies 1-4). Altogether,

159   this selective bactericidal activity of macrolides and tetracyclines on specific gut commensals

160   could provide an explanation for the strong effects these drug classes have on the gut

161   microbiota composition of human individuals. The gut microbes killed from the drug would be

162   inadvertently removed from community, whereas the ones being only inhibited could recover

163   when the therapy stops.

164   Knowing that drug combinations often have species-specific outcomes[12], we

165   reasoned that we could identify drugs that selectively antagonize the effect of antibiotics on

166   gut microbes, while retaining activity against pathogens. Therefore, we screened the

167   Prestwick library to identify antagonizing compounds to erythromycin or doxycycline on two

168   abundant and prevalent gut microbes, *B. vulgatus* and *B. uniformis* (Fig. 3a, Extended Data

169   Fig. 9). Of the 19 identified hits (Fig. 3b, Suppl. Table 4), we tested the 14 candidates with

170   the strongest activity in a concentration-dependent manner (Extended Data Fig. 10a). Nine

171   retained antagonistic activity over a broader concentration range, which we confirmed by

172   checkerboard assays (Fig. 3c). The antidotes that showed the strongest antagonisms were

173   the anticoagulant drug dicumarol, and two non-steroidal anti-inflammatory drugs, tolfenamic

174   acid and diflunisal. While dicumarol rescued *B. vulgatus* from erythromycin and diflunisal

175   from doxycycline, tolfenamic acid was able to protect *B. vulgatus* from both drugs. In

176   addition, these interactions were able to at least partially rescue the killing of *B. vulgatus* by

177   erythromycin and doxycycline (Extended Data Fig. 10b). We then probed two of these drugs

178   for their ability to protect other abundant gut commensals and confirmed that both dicumarol

179   and tolfenamic acid were able to counteract erythromycin on several species (Fig. 3d,

180   Extended Data Fig. 11). In contrast, both drugs did not affect the potency of erythromycin on

181   *Staphylococcus aureus, Streptococcus pneumoniae* and *Enterococcus faecium*, pathogens

182   against which erythromycin is active/prescribed (Fig. 3e, Extended Data Fig. 12a). For

183   example, tolfenamic acid and dicumarol at concentration ranges of 5-40 μM could rescue the

184   growth of five out of seven tested abundant gut commensal species at clinically relevant

185   erythromycin concentrations (Fig. 3f, Extended Data Fig. 12b). Altogether, our data provides

186   a proof-of-principle for identifying antidotes that specifically mask the collateral damage of

187   antibiotics on commensals. This concept would need to be further validated in the future in

188   animal models. Antidotes may also need to be modified to late (colon)-release or non-

189   absorbable formulations to ensure they reach the gut and to minimize adverse effects from

190   their primary action.

191   In summary, our study provides a high-resolution map of the collateral damage of

192   antibiotics on 50 different resident gut microbes down to the level of individual drugs, species

193   and partially even strains. We challenge the universal divide of antibiotics into bacteriostatic

194   and bactericidal across bacteria, as this breaks down when tested beyond model organisms.

195   Antibiotics with preferential killing of some species may be the most detrimental to our gut

196   flora, although the first studies in a few healthy individuals point to the gut microbiota having

197   some resilience against specific antibiotic regimens[44]. Understanding the underlying

198   mechanisms for this selective killing might open up ways for the development of new

199   antimicrobials, but also strategies for controlled microbiome modulation[15]. Finally, we provide

200   a proof-of-concept that species-specificity of drug combinations[12] can be exploited to identify

201   antidotes that selectively protect the gut microbiota from the adverse effects of systemic

202   antibiotic therapy. This new approach adds to proposed and existing strategies of gut

203   microbiota protection against antibiotics, such as co-administration of activated charcoal[45], β-

204   lactamases[46], probiotics or (autologous) fecal transplants[47]. Overall, our results suggest that

205   interactions of antibiotics and commensals merit deeper exploration, as our current

206   knowledge of the mode(s) of action of antibiotics in model pathogens is not necessarily

207   transferable to commensals.

8

208 **METHODS**

209 **Growth conditions**

210 All experiments from this study were performed in an anaerobic chamber (Coy Laboratory

211 Products Inc) (2% H_2, 12% CO_2, 86% N_2) and all materials and solutions used for these

212 experiments were pre-reduced for at least 24 h before use unless specified otherwise.

213 Bacteria used in this study were typically pre-cultured for two overnights: Cells were cultured

214 in 5 ml modified Gifu Anaerobic Medium broth (MGAM) (HyServe GmbH & Co.KG, Germany,

215 produced by Nissui Pharmaceuticals) and grown at 37°C overnight. The next day, cells were

216 diluted 1/100 in 5 ml MGAM medium and grown at 37°C for a second overnight before

217 starting the experiments.

218

219 **Quantitative assay for minimum inhibitory concentration determination with MICs test**

220 **strips**

221 MICs test strips were purchased from Liofilchem or Oxoid (Suppl. Table 2). All MICs were

222 measured under anaerobic growth conditions inside a Coy anaerobic chamber. Bacteria

223 were precultured in MGAM for two overnights and cultures were diluted to OD_{578} = 0.5. 50 µl

224 of the diluted culture were spread on a MGAM agar plate and allowed to dry for 15 min. The

225 MIC test strip was placed on the agar with sterile tweezers, allowing the part with the lowest

226 concentration touch the agar first. Plates were incubated at 37°C inside the anaerobic

227 chamber, at least overnight and longer depending on the species-specific growth

228 requirements. After formation of a symmetrical inhibition ellipse, plates were taken out of the

229 chamber and imaged under controlled lighting conditions (spImager S&P Robotics Inc.) using

230 an 18 megapixel Canon Rebel T3i (Canon Inc. USA). MICs were directly determined from

231 the strip scale at the point where the edge of the inhibition ellipse intersects the MIC test

232 strip. All MICs were determined in duplicates. In cases of an eight-fold difference between

233 the two values, a third replicate was done. In all cases, this resulted in a clear outlier (> 8-fold

234 different from other two MICs) that was removed from the dataset.

235

9

MIC comparison to ChEMBL and EUCAST databases

Previously known MICs were extracted from the ChEMBL database (version 24)[27] and EUCAST (obtained on May 14, 2018)[24]. Antibiotics from these two datasets were mapped to our dataset by name. Species were mapped using NCBI Taxonomy Identifiers and species names. For MICs from ChEMBL, a keyword-based approach was used to exclude experiments on species with mutations, deletions, insertions, etc. The EUCAST database contains a large number of reported MICs for each compound–species pair. We collapsed these to a single value by calculating the median MIC.

Estimates on the abundance and prevalence of species in the healthy human gut microbiome were calculated using mOTUs v2[48] as follows: Relative species abundances were determined in 727 shotgun metagenomic samples from donors in the control groups of multiple studies from various countries and continents[49-53]. Prior to taxonomic profiling, metagenomes were quality controlled using the MOCAT2 -rtf procedure[54], which removed reads with ≥95% sequence identity and an alignment length of ≥45bp to the human genome hg19. Taxonomic profiles were then created using mOTUs version 2.1.0[48] with parameters -l 75 ; -g 2; and -c. Afterwards relative abundances below 10^{-4} were set to zero and species with nonzero abundance in <5 samples discarded. For the retained 1,350 species, prevalence was defined as the percentage of samples with nonzero abundance; a prevalence cut-off of 1% was chosen to classify species into "rare" and "common" species. For all species in the MIC dataset, we manually assessed their status as pathogenic or non-pathogenic species using encyclopaedic and literature knowledge. Pathogenic species that occur in more than 1% of healthy people (i.e. are designated as "common") were classified as "potentially pathogenic species" that can, for example, cause diseases in immunocompromised patients.

Killing curves and survival assay

Cells were precultured as described in the *growth conditions* section before being diluted to an $OD_{578}=0.01$ and grown for 2 h at 37°C (unless specified otherwise). Next, cells were

264   diluted 1/2 in MGAM containing a 10-fold MIC of erythromycin, azithromycin or doxycycline

265   (final antibiotic concentration is 5-fold MIC) and incubated in the presence of the antibiotic for

266   5 h at 37°C. At several time-points (0, 1h, 2h, 3h, 4h, 5h), 100 μl of cells were serial-diluted in

267   PBS (10^{-1} to 10^{-8} dilutions) and plated on MGAM-Agar plates for CFU counting. When no

268   cells were detected using this method, a bigger volume of culture (up to 2 ml) was plated to

269   be able to detect CFUs. Agar plates were incubated overnight at 37°C and colonies were

270   counted the next day, either manually, for low CFU numbers, or using the *Analyze Particles*

271   tool from ImageJ[55].

272

273   **Live/dead staining**

274   Cells were precultured as described in the *growth conditions* section before being diluted to

275   an OD_{578}=0.01 and grown for 2 h at 37°C. Cells were next diluted 1/2 in MGAM containing

276   10-fold MIC of erythromycin, azithromycin or doxycycline (final concentration is 5-fold the

277   MIC) and incubated in the presence of the antibiotic for 5 h at 37°C. Then, cells were

278   live/dead stained using the *LIVE/DEAD BacLight Bacterial viability and counting kit* (#L34856

279   Molecular Probes, ThermoFisher) according to the manufacturer's protocol before and after

280   antibiotic treatment.

281

282   **Flow cytometry**

283   Stained cells were counted using a BD LSRFortessa[TM] flow cytometer. The forward and side

284   scatter signals (488 nm) as well as the green and red fluorescent signals (488-530/30A filter

285   and 561-610/20A filter, respectively) were acquired. The FSC/SSC detectors were set to

286   logarithmic scale. The flow rate varied between 12 μl/min and 60 μl/min depending on the

287   concentration of each sample, and the analysis was stopped when 10,000 target events

288   were measured. Graphs were generated using the FlowJo V10.3 software (Treestar).

289

290   **Microscopy**

291   For live/dead imaging, stained cells were washed twice in 0.85% NaCl before being spotted

292   on 0.85% NaCl +1% agarose pads between a glass slide and a coverslip. For time-lapse

293   imaging, cells were precultured as described in the *growth conditions* section. Cells were

294   then diluted to an OD_{578}=0.01 and grown for 3 h at 37°C before being spotted on MGAM

295   +1% agarose pads, supplemented or not with 15 µg/ml erythromycin (5-fold MIC) between a

296   glass slide and a coverslip. Slides were sealed with valap (to avoid/delay oxygen

297   permeation) and taken outside of the anaerobic chamber for imaging. In these conditions,

298   untreated bacteria kept growing rapidly (Movie 1 + 3). The imaging was performed using a

299   Nikon Eclipse Ti inverted microscope, equipped with a Nikon DS-Qi2 camera, a Nikon Plan

300   Apo Lambda 60X oil Ph3 DM phase contrast objective and a Nikon HC mCherry filter set (Ex

301   562/40; DM 593; BA 641/75) to detect propidium iodide fluorescence. Images were acquired

302   with the NIS-Elements AR4.50.00 software and processed with Fiji v.2.0.0-rc-68/1.52h[56].

303

304   **Growth curves**

305   Cells were precultured as described in the *growth conditions* section. Then, cells were diluted

306   to an OD_{578}=0.01 in a 96-well plate sealed with a breathable membrane (Breathe-Easy®)

307   and grown for 2 h. Next, erythromycin was added to the culture to a final concentration of 15

308   µg/ml (5-fold MIC) and growth curves were acquired for 20 h using a microplate

309   spectrophotometer (EON, Biotek) by measuring the OD_{578} every hour after 30 sec of linear

310   shaking.

311

312   **Screen for microbiome-protective antibiotic antagonism**

313   *Preparation of screening plates.* The Prestwick Chemical Library was purchased from

314   Prestwick Chemical Inc. and drugs were re-arrayed, diluted and stored in 96 well format as

315   described before[4]. We prepared drug plates (2 x drug concentration) in MGAM medium and

316   stored them at -30°C. For each experiment, drug plates were thawed, supplemented with the

317   respective antibiotic solution (freshly prepared in MGAM) and pre-reduced in the anaerobic

12

318   chamber overnight. All rearranging and aliquoting steps were done using the Biomek FXP

319   (Beckman Coulter) system.

320   *Inoculation and screening conditions*. Strains were grown twice overnight, the second

321   overnight culture was diluted in MGAM to reach $OD_{578\ nm}$ 0.04 (4 x the desired starting OD).

322   25 µl of the diluted cultures were used to inoculate wells containing 50 µl of 2x concentrated

323   Prestwick drug and 25 µl of the 4x concentrated antibiotic using the semi-automated, 96-well

324   multi-channel pipette ep*Motion*96 (Eppendorf). Each well contained 1% DMSO, 20 µM of the

325   Prestwick drug and a species-specific antibiotic concentration that was just inhibitory for the

326   respective strain (0.625 µM for erythromycin, 0.04 µM doxycycline for *B. uniformis* and 0.08

327   µM doxycycline for *B. vulgatus*). Plates were sealed with breathable membranes (Breathe-

328   Easy®) and OD_{578} was measured hourly after 30 sec of linear shaking with a microplate

329   spectrophotometer (EON, Biotek) and an automated microplate stacker (Biostack 4, Biotek)

330   fitted inside a custom-made incubator (EMBL Mechanical Workshop). Growth curves were

331   collected up to 24 h. For each antibiotic, each species was screen in biological duplicates. All

332   experiments included control wells of unperturbed growth (32 wells per run) and control wells

333   for growth in the presence of the antibiotic only (8 wells per plate).

334   *Analysis pipeline and hit calling*. All growth curves within a plate were truncated at the

335   transition time from exponential to stationary phase and converted to normalized AUCs using

336   in-run control wells (no drug) as described before[4] .We then calculated z-scores based on

337   these normalized AUCs, removed replicates with 8-fold differences in z-scores to eliminate

338   noise effects, computed mean z- scores across the two replicates and selected combinations

339   with mean z-scores > 3. This selection included 19 potential antibiotic antagonists and we

340   followed up on 14 of them (7 potential erythromycin and 7 potential doxycycline antagonists

341   in either *B. vulgatus* or *B. uniformis* – see Extended Data Fig. 9) in independent experiments.

342   *Validation of microbiome-protective antagonists.* First, we kept the erythromycin/doxycycline

343   concentration constant (0.625 µM for erythromycin, 0.078 µM (*B. vulgatus*)/ 0.039 µM (*B.*

344   *uniformis*) for doxycycline) and tested concentration gradients of the potential antagonists

345   with ranges depending on the antagonist's solubility. Compounds were purchased from

13

346   independent vendors (Suppl. Table 5) and dissolved at 100x starting concentration in DMSO.

347   Eight 2-fold serial dilutions were prepared in 96-well plates with each row containing a

348   different antagonist, sufficient control DMSO wells and wells with just the respective antibiotic

349   ('antibiotic-only' control). These master plates were diluted in MGAM medium (50 µl) to 2 x

350   assay concentration and 25 µl freshly prepared antibiotic solution (4x test concentration) was

351   added. Plates were pre-reduced overnight in an anaerobic chamber and inoculated with 25

352   µl of overnight cultures (prepared as described under *Growth conditions*) to reach a starting

353   OD_{578} of 0.01 and 1% DMSO concentration. Growth was monitored hourly for 24 h after 30

354   sec of linear shaking (as described for the screen[4]). Experiments were performed in

355   biological triplicates. For analysis, growth curves were converted into normalized AUCs (see

356   above). We accounted for residual growth in the presence of the antibiotic by subtracting the

357   median normalized AUCs of the 'antibiotic-only' control per plate. We computed medians

358   across triplicates and considered a normalized AUC > 0.25 as concentration-dependent

359   growth rescue by the antagonist.

360   *Checkerboard assays for anaerobic commensals.* Validated antagonists were further

361   investigated in 8x8 checkerboard assays, where both antibiotics and antagonists were

362   titrated against each other. Such assays were first performed for the commensals that were

363   originally screened (i. e. *B. vulgatus* and *B. uniformis* – 4 replicates) and later expanded

364   towards six further gut microbes (*B. caccae*, *B. fragilis* NT, *B. ovatus*, *B. thetaiotaomicron*, *P.*

365   *copri*, *P. distasonis* – 2 replicates). For vertical gradients, 2-fold serial dilutions of the

366   antagonists were prepared first in 100x in DMSO and diluted in MGAM as described above

367   (section 'Validation of microbiome-protective antagonists'). Horizontal antibiotic dilution

368   series were freshly prepared in MGAM at 4x final concentration in equidistant concentration

369   steps. Both, vertical and horizontal dilution series were combined (50 µl of the antagonist

370   gradients (2x) and 25 µl of the antibiotic gradients (4x)) in 96 well plates. Plates were pre-

371   reduced under anaerobic conditions overnight, inoculated with 25 µl of diluted overnight

372   culture (at 4x starting OD) and sealed with breathable membrane (Breathe-Easy®). Bacterial

373   growth was monitored once per hour for 24 h after 30 sec linear shaking (Eon + Biostack 4,

374 Biotek) under anaerobic conditions. Growth curves were converted into normalized AUCs as

375 described using in-plate controls to define unperturbed growth.

376 *Checkerboard assays for pathogens under aerobic conditions.* For three pathogens (*S.*

377 *aureus* DSM20231 ATCC 12600 and *E. faecium* ATCC19434) 8x8 checkerboard assays

378 were performed in transparent 384 well plates (Greiner BioOne GmbH), with each well

379 containing a total volume of 30 µl in total for *S. aureus* and 55 µl for *E. faecium*. *S. aureus*

380 strains were grown in tryptic soy broth (TSB, Sigma Aldrich), *E. faecium* in BHI medium

381 (Sigma Aldrich). Drugs were arrayed in 2-fold serial dilutions for the checkerboards. Cell

382 were inoculated at initial OD_{595nm} ~0.01 from an overnight culture. Plates were sealed with

383 breathable membranes (Breathe-Easy), incubated at 37°C (Cytomat 2, Thermo Scientific)

384 with continuous shaking and OD_{595nm} was measured every 30 min for 16 h in a Filtermax F5

385 multimode plate reader (Molecular Devices). For *S. pneumoniae* D39, we only tested

386 concentration gradients of the potential antagonists in a constant antibiotic concentration (0.2

387 µM erythromycin) in BHI medium. All experiments were done at least in 2 biological

388 replicates and 2 technical replicates. Wells in which there was significant condensation were

389 removed and background due to medium was subtracted. Growth curves were trimmed at

390 the transition to stationary phase (9 h for *S. aureus*, 12 h for *E. faecium*). AUCs were

391 calculated and normalised by the median of the internal no-drug control wells (n = 6).

392 Interactions were quantified according to the Bliss interaction model[57]. Interactions were

393 called antagonistic if the median of all the interaction scores for a given checkerboard was

394 above 0.05, synergistic if the value was below -0.05 and neutral if lying between these two

395 cut-offs.

396

397 **Phylogenetic analysis/phylogenetic tree construction**

398 In order to generate a phylogenetic tree for the different isolates, the nucleotide sequences

399 for a set of universally occurring, protein coding, single copy phylogenetic marker genes[48,58]

400 were extracted from reference genomes or genome assemblies using fetchMG[58]

401 (https://motu-tool.org/fetchMG.html). Within the framework of the ete3 toolkit[59],

15

402   ClustalOmega[60] was used to create sequence alignments for each marker gene

403   independently and all columns with more than 10% gaps were removed. The individual

404   alignments were concatenated and finally, a phylogenetic tree was inferred from the

405   combined alignment using IQTree[61].

406

407   **Data availability**

408   Data is available upon request.

409

410   **Code availability**

411   Code is available upon request.

412

413

16

REFERENCES

1   Blaser, M. J. Antibiotic use and its consequences for the normal microbiome. *Science* **352**, 544-545, doi:10.1126/science.aad9358 (2016).

2   Modi, S. R., Collins, J. J. & Relman, D. A. Antibiotics and the gut microbiota. *J Clin Invest* **124**, 4212-4218, doi:10.1172/JCI72333 (2014).

3   Becattini, S., Taur, Y. & Pamer, E. G. Antibiotic-Induced Changes in the Intestinal Microbiota and Disease. *Trends Mol Med* **22**, 458-478, doi:10.1016/j.molmed.2016.04.003 (2016).

4   Maier, L. *et al.* Extensive impact of non-antibiotic drugs on human gut bacteria. *Nature* **555**, 623-628, doi:10.1038/nature25979 (2018).

5   Cho, I. *et al.* Antibiotics in early life alter the murine colonic microbiome and adiposity. *Nature* **488**, 621-626, doi:10.1038/nature11400 (2012).

6   Cox, L. M. *et al.* Altering the intestinal microbiota during a critical developmental window has lasting metabolic consequences. *Cell* **158**, 705-721, doi:10.1016/j.cell.2014.05.052 (2014).

7   Nobel, Y. R. *et al.* Metabolic and metagenomic outcomes from early-life pulsed antibiotic treatment. *Nat Commun* **6**, 7486, doi:10.1038/ncomms8486 (2015).

8   Ruiz, V. E. *et al.* A single early-in-life macrolide course has lasting effects on murine microbial network topology and immunity. *Nat Commun* **8**, 518, doi:10.1038/s41467-017-00531-6 (2017).

9   Hirsch, A. G. *et al.* Early-life antibiotic use and subsequent diagnosis of food allergy and allergic diseases. *Clin Exp Allergy* **47**, 236-244, doi:10.1111/cea.12807 (2017).

10   Korpela, K. *et al.* Intestinal microbiome is related to lifetime antibiotic use in Finnish pre-school children. *Nat Commun* **7**, 10410, doi:10.1038/ncomms10410 (2016).

11   Parker, E. P. K. *et al.* Changes in the intestinal microbiota following the administration of azithromycin in a randomised placebo-controlled trial among infants in south India. *Sci Rep* **7**, 9168, doi:10.1038/s41598-017-06862-0 (2017).

12   Brochado, A. R. *et al.* Species-specific activity of antibacterial drug combinations. *Nature* **559**, 259-263, doi:10.1038/s41586-018-0278-9 (2018).

13   Falony, G. *et al.* Population-level analysis of gut microbiome variation. *Science* **352**, 560-564, doi:10.1126/science.aad3503 (2016).

14   Rothschild, D. *et al.* Environment dominates over host genetics in shaping human gut microbiota. *Nature* **555**, 210-215, doi:10.1038/nature25973 (2018).

15   Schmidt, T. S. B., Raes, J. & Bork, P. The Human Gut Microbiome: From Association to Modulation. *Cell* **172**, 1198-1215, doi:10.1016/j.cell.2018.02.044 (2018).

16   Jackson, M. A. *et al.* Gut microbiota associations with common diseases and prescription medications in a population-based cohort. *Nat Commun* **9**, 2655, doi:10.1038/s41467-018-05184-7 (2018).

17   Maier, L. & Typas, A. Systematically investigating the impact of medication on the gut microbiome. *Curr Opin Microbiol* **39**, 128-135, doi:10.1016/j.mib.2017.11.001 (2017).

18   Kuhn, M., Letunic, I., Jensen, L. J. & Bork, P. The SIDER database of drugs and side effects. *Nucleic Acids Res* **44**, D1075-1079, doi:10.1093/nar/gkv1075 (2016).

19   Arrieta, M. C. *et al.* Early infancy microbial and metabolic alterations affect risk of childhood asthma. *Sci Transl Med* **7**, 307ra152, doi:10.1126/scitranslmed.aab2271 (2015).

20   Dethlefsen, L. & Relman, D. A. Incomplete recovery and individualized responses of the human distal gut microbiota to repeated antibiotic perturbation. *Proc Natl Acad Sci U S A* **108 Suppl 1**, 4554-4561, doi:10.1073/pnas.1000087107 (2011).

21   Saari, A., Virta, L. J., Sankilampi, U., Dunkel, L. & Saxen, H. Antibiotic exposure in infancy and risk of being overweight in the first 24 months of life. *Pediatrics* **135**, 617-626, doi:10.1542/peds.2014-3407 (2015).

22   Gajdacs, M., Spengler, G. & Urban, E. Identification and Antimicrobial Susceptibility Testing of Anaerobic Bacteria: Rubik's Cube of Clinical Microbiology? *Antibiotics (Basel)* **6**, doi:10.3390/antibiotics6040025 (2017).

468 23   Nagy, E., Boyanova, L., Justesen, U. S. & Infections, E. S. G. o. A. How to isolate,
469   identify and determine antimicrobial susceptibility of anaerobic bacteria in routine
470   laboratories. *Clin Microbiol Infect* **24**, 1139-1148, doi:10.1016/j.cmi.2018.02.008
471   (2018).
472 24   The European Committee on Antimicrobial Susceptibility Testing. Breakpoint tables
473   for interpretation of MICs and zone diameters, v., 2019.
474   http://www.eucast.org/clinical_breakpoints/. .
475 25   Bullman, S. *et al.* Analysis of Fusobacterium persistence and antibiotic response in
476   colorectal cancer. *Science* **358**, 1443-1448, doi:10.1126/science.aal5240 (2017).
477 26   Manfredo Vieira, S. *et al.* Translocation of a gut pathobiont drives autoimmunity in
478   mice and humans. *Science* **359**, 1156-1161, doi:10.1126/science.aar7201 (2018).
479 27   Gaulton, A. *et al.* The ChEMBL database in 2017. *Nucleic Acids Res* **45**, D945-D954,
480   doi:10.1093/nar/gkw1074 (2017).
481 28   Bryan, L. E., Kowand, S. K. & Van Den Elzen, H. M. Mechanism of aminoglycoside
482   antibiotic resistance in anaerobic bacteria: Clostridium perfringens and Bacteroides
483   fragilis. *Antimicrob Agents Chemother* **15**, 7-13, doi:10.1128/aac.15.1.7 (1979).
484 29   Cani, P. D. & de Vos, W. M. Next-Generation Beneficial Microbes: The Case of
485   Akkermansia muciniphila. *Front Microbiol* **8**, 1765, doi:10.3389/fmicb.2017.01765
486   (2017).
487 30   Routy, B. *et al.* Gut microbiome influences efficacy of PD-1-based immunotherapy
488   against epithelial tumors. *Science* **359**, 91-97, doi:10.1126/science.aan3706 (2018).
489 31   Slimings, C. & Riley, T. V. Antibiotics and hospital-acquired Clostridium difficile
490   infection: update of systematic review and meta-analysis. *J Antimicrob Chemother*
491   **69**, 881-891, doi:10.1093/jac/dkt477 (2014).
492 32   Baron, S., Diene, S. & Rolain, J.-M. Human microbiomes and antibiotic resistance.
493   *Human Microbiome Journal* (2018).
494 33   Tramontano, M. *et al.* Nutritional preferences of human gut bacteria reveal their
495   metabolic idiosyncrasies. *Nat Microbiol* **3**, 514-522, doi:10.1038/s41564-018-0123-9
496   (2018).
497 34   Cohen J, O. S. M., Powderly W G, editors. . *Infectious diseases.2 vol. 3rd ed. St.
498   Louis, Mo.; London: Mosby*. (2010.).
499 35   Habib, G. *et al.* 2015 ESC Guidelines for the management of infective endocarditis:
500   The Task Force for the Management of Infective Endocarditis of the European
501   Society of Cardiology (ESC). Endorsed by: European Association for Cardio-Thoracic
502   Surgery (EACTS), the European Association of Nuclear Medicine (EANM). *Eur Heart
503   J* **36**, 3075-3128, doi:10.1093/eurheartj/ehv319 (2015).
504 36   Kasper DL, F. A., Hauser SL, Longo DL. *Harrison's Principles of Internal Medicine,
505   18e, 2012 McGraw-Hill*.
506 37   Liang, S. Y. & Kumar, A. Empiric antimicrobial therapy in severe sepsis and septic
507   shock: optimizing pathogen clearance. *Curr Infect Dis Rep* **17**, 493,
508   doi:10.1007/s11908-015-0493-6 (2015).
509 38   Lobritz, M. A. *et al.* Antibiotic efficacy is linked to bacterial cellular respiration. *Proc
510   Natl Acad Sci U S A* **112**, 8173-8180, doi:10.1073/pnas.1509743112 (2015).
511 39   Ocampo, P. S. *et al.* Antagonism between bacteriostatic and bactericidal antibiotics is
512   prevalent. *Antimicrob Agents Chemother* **58**, 4573-4582, doi:10.1128/AAC.02463-14
513   (2014).
514 40   French, G. L. Bactericidal agents in the treatment of MRSA infections--the potential
515   role of daptomycin. *J Antimicrob Chemother* **58**, 1107-1117, doi:10.1093/jac/dkl393
516   (2006).
517 41   Jelic, D. & Antolovic, R. From Erythromycin to Azithromycin and New Potential
518   Ribosome-Binding Antimicrobials. *Antibiotics (Basel)* **5**,
519   doi:10.3390/antibiotics5030029 (2016).
520 42   Nemeth, J., Oesch, G. & Kuster, S. P. Bacteriostatic versus bactericidal antibiotics for
521   patients with serious bacterial infections: systematic review and meta-analysis. *J
522   Antimicrob Chemother* **70**, 382-395, doi:10.1093/jac/dku379 (2015).

523 43 Wald-Dickler, N., Holtom, P. & Spellberg, B. Busting the Myth of "Static vs Cidal": A
524   Systemic Literature Review. *Clin Infect Dis* **66**, 1470-1474, doi:10.1093/cid/cix1127
525   (2018).
526 44 Palleja, A. *et al.* Recovery of gut microbiota of healthy adults following antibiotic
527   exposure. *Nat Microbiol* **3**, 1255-1265, doi:10.1038/s41564-018-0257-9 (2018).
528 45 de Gunzburg, J. *et al.* Protection of the Human Gut Microbiome From Antibiotics. *The
529   Journal of Infectious Diseases* **217**, 628-636, doi:10.1093/infdis/jix604 (2017).
530 46 Stiefel, U., Nerandzic, M. M., Koski, P. & Donskey, C. J. Orally administered beta-
531   lactamase enzymes represent a novel strategy to prevent colonization by Clostridium
532   difficile. *J Antimicrob Chemother* **62**, 1105-1108, doi:10.1093/jac/dkn298 (2008).
533 47 Suez, J. *et al.* Post-Antibiotic Gut Mucosal Microbiome Reconstitution Is Impaired by
534   Probiotics and Improved by Autologous FMT. *Cell* **174**, 1406-1423 e1416,
535   doi:10.1016/j.cell.2018.08.047 (2018).
536 48 Milanese, A. *et al.* Microbial abundance, activity and population genomic profiling with
537   mOTUs2. *Nat Commun* **10**, 1014, doi:10.1038/s41467-019-08844-4 (2019).
538 49 Feng, Q. *et al.* Gut microbiome development along the colorectal adenoma-
539   carcinoma sequence. *Nat Commun* **6**, 6528, doi:10.1038/ncomms7528 (2015).
540 50 Vogtmann, E. *et al.* Colorectal Cancer and the Human Gut Microbiome:
541   Reproducibility with Whole-Genome Shotgun Sequencing. *PLoS One* **11**, e0155362,
542   doi:10.1371/journal.pone.0155362 (2016).
543 51 Wirbel, J. *et al.* Meta-analysis of fecal metagenomes reveals global microbial
544   signatures that are specific for colorectal cancer. *Nat Med* **25**, 679-689,
545   doi:10.1038/s41591-019-0406-6 (2019).
546 52 Yu, J. *et al.* Metagenomic analysis of faecal microbiome as a tool towards targeted
547   non-invasive biomarkers for colorectal cancer. *Gut* **66**, 70-78, doi:10.1136/gutjnl-
548   2015-309800 (2017).
549 53 Zeller, G. *et al.* Potential of fecal microbiota for early-stage detection of colorectal
550   cancer. *Mol Syst Biol* **10**, 766, doi:10.15252/msb.20145645 (2014).
551 54 Kultima, J. R. *et al.* MOCAT2: a metagenomic assembly, annotation and profiling
552   framework. *Bioinformatics* **32**, 2520-2523, doi:10.1093/bioinformatics/btw183 (2016).
553 55 Schneider, C. A., Rasband, W. S. & Eliceiri, K. W. NIH Image to ImageJ: 25 years of
554   image analysis. *Nat Methods* **9**, 671-675 (2012).
555 56 Schindelin, J. *et al.* Fiji: an open-source platform for biological-image analysis. *Nat
556   Methods* **9**, 676-682, doi:10.1038/nmeth.2019 (2012).
557 57 CI, B. The toxicity of poisons applied jointly. *Ann Appl Biol* **26**, 585-615 (1939).
558 58 Sunagawa, S. *et al.* Metagenomic species profiling using universal phylogenetic
559   marker genes. *Nat Methods* **10**, 1196-1199, doi:10.1038/nmeth.2693 (2013).
560 59 Huerta-Cepas, J., Serra, F. & Bork, P. ETE 3: Reconstruction, Analysis, and
561   Visualization of Phylogenomic Data. *Mol Biol Evol* **33**, 1635-1638,
562   doi:10.1093/molbev/msw046 (2016).
563 60 Sievers, F. *et al.* Fast, scalable generation of high-quality protein multiple sequence
564   alignments using Clustal Omega. *Mol Syst Biol* **7**, 539, doi:10.1038/msb.2011.75
565   (2011).
566 61 Nguyen, L. T., Schmidt, H. A., von Haeseler, A. & Minh, B. Q. IQ-TREE: a fast and
567   effective stochastic algorithm for estimating maximum-likelihood phylogenies. *Mol
568   Biol Evol* **32**, 268-274, doi:10.1093/molbev/msu300 (2015).
569
570
571

572 **SUPPLEMENTARY INFORMATION**

573 **Supplementary tables**

574 **Supplementary Table 1**

575 Annotation and classification of antibiotics

576 **Supplementary Table 2**

577 MICs strips used in this study

578 **Supplementary Table 3**

579 MICs as determined by MIC strips for selected antibiotics

580 **Supplementary Table 4**

581 Hitlist: Screen for microbiome-protective antagonists to erythromycin/tetracycline

582 **Supplementary Table 5**

583 Compounds used in this study

584 **Supplementary movies**

585 **Movie 1**

586 Time-lapse of *B. vulgatus* growing on MGAM-Agarose 1% pad.

587 **Movie 2**

588 Time-lapse of *B. vulgatus* growing on MGAM-Agarose 1% pad containing 5-fold MIC of

589 erythromycin.

590 **Movie 3**

591 Time-lapse of *B. uniformis* growing on MGAM-Agarose 1% pad.

592 **Movie 4**

593 Time-lapse of *B. uniformis* growing on MGAM-Agarose 1% pad containing 5-fold MIC of

594 erythromycin.

595

605

606

Author contributions

608   This study was conceived by KRP, PB and AT; designed by LM, CVG, MP and AT; and

609   supervised by LM and AT. Experiments were conducted by LM, CVG and MP. TB and EEA

610   contributed to MIC measurements and EC to checkerboard analyses. Data preprocessing,

611   curation and comparisons to existing databases were performed by JW, MK, AM, UL, SKF

612   and GZ. Data interpretation was performed by LM, CVG, JW, GZ and AT. LM, CVG and AT

613   wrote the manuscript with feedback from all authors; LM, CVG, JW and MK designed figures

614   with inputs from GZ and AT. All authors approved the final version for publication.

615

Author information

617   EMBL has filed a patent application on using the antidotes identified in this study for

618   prevention and/or treatment of dysbiosis and for microbiome protection (European patent

619   application number EP19216548.8). LM, CVG, EC and AT are listed as inventors.

620   Correspondence and requests for materials should be addressed to typas@embl.de or

621   l.maier@uni-tuebingen.de.

622

623
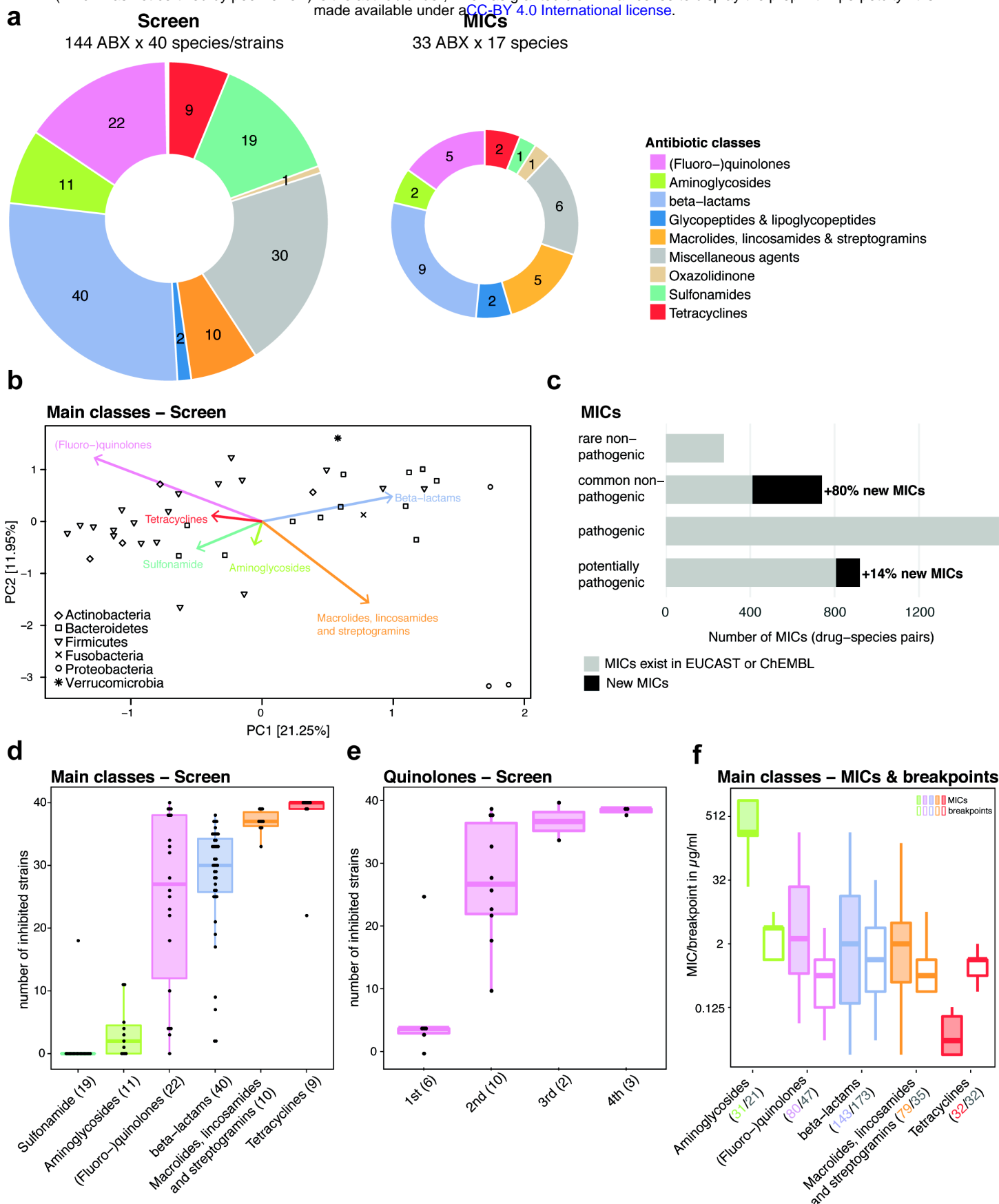
**Figure 1 – Activity spectrum of antibiotic classes on human gut commensals.**
a. Overview of antibiotics tested in initial screen at 20 μM concentration[4] and validated by MIC determination in this study. **b.** Principal component analysis based on AUCs from the initial screen on the effects of antibiotics on gut commensals. Antibiotic classes drive some separation at the phylum level, e.g. beta-lactams separate Bacteroidetes and macrolides/lincosamides/streptogramins separate Proteobacteria. **c.** Comparison of MICs from this study to MICs available from public databases. Species are classified as "common" or "rare" if they are present in the gut microbiome of more or less than 1% of 727 healthy individuals, respectively (see Methods). **d.** For the main antibiotic classes from the screen, the numbers of inhibited strains are shown (N as in **a**). 40 strains tested in total at a 20 μM antibiotic concentration. Boxes span the IQR and whiskers extend to the most extreme data points up to a max of 1.5 times the IQR. **e.** Number of inhibited strains per (fluoro-)quinolone drug generation. Number of tested drugs per generation is indicated in brackets on x-axis labeling. Boxplots as in panel **d**. **f.** MICs of drug-species pairs for the main antibiotic classes measured in this study are depicted next to EUCAST clinical (susceptibility) breakpoints for pathogens. Numbers of drug-species pairs (MICs; colored) and of antibiotic per class (EUCAST clinical breakpoints; grey) are shown in brackets. Boxplots as in panel, **d**, y-axis is log2 scale.
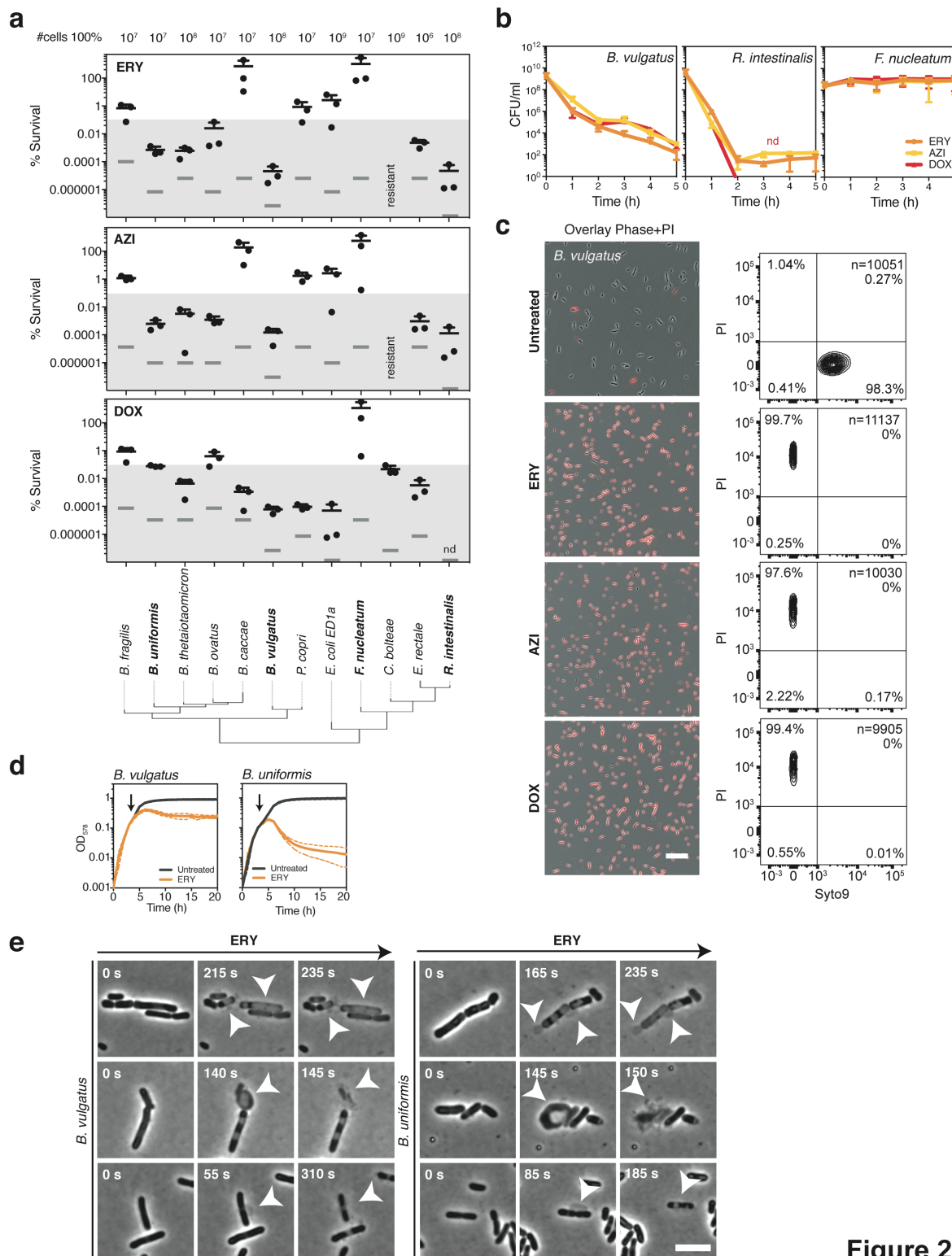
Figure 2

Figure 2 - Macrolides and tetracyclines kill human gut commensal species

a. The survival of 12 abundant gut microbe species was measured after a 5-hour treatment with a 5-fold MIC of erythromycin (ERY), azithromycin (AZI) or doxycycline (DOX). The survival was assessed by counting CFUs/ml before and after antibiotic treatment. The number of CFUs/ml before treatment was set as 100%. The detection limit for each experiment (gray bar) and the bactericidal threshold (shaded area) are indicated. Species are plotted according to phylogeny (IQTree, Methods) and in bold are noted the species that are used in later panels. The graph shows the mean+SD of 3 independent experiments. **b.** Time-kill curves of *B. vulgatus*, *R. intestinalis* and *F. nucleatum* after antibiotic treatments. Survival was assessed by CFU counting over a 5 hour-treatment of ERY, AZI or DOX. This graph shows the mean±SD of 3 independent experiments. Nd: non-detectable. Time-kill curves for the other tested gut microbes can be found in Extended Data Fig. 5. **c.** Live/dead staining of macrolide or tetracycline-treated *B. vulgatus*. The left panel shows an overlay of phase contrast and fluorescence microscopy images of propidium iodide (PI)-stained *B. vulgatus* before and 5 hours after ERY, AZI or DOX treatment. Cultures were concentrated before imaging; the scale bar is 10 μm. The right panel shows the corresponding quantification of live/dead-stained cells by flow cytometry with Syto9 on the x-axis (live cells) and PI on the y-axis (dead cells). Both the total number of measured events (n) and the percentage of cells found in each quadrant are indicated. **d.** Erythromycin induces lysis of *B. vulgatus* and *B. uniformis*. *B. vulgatus* and *B. uniformis* were grown for 3 hours before addition (yellow) or not (black) of 15 μg/ml ERY treatment (5-fold MIC; yellow) as indicated by the arrow. Growth curves were acquired for 20 hours. This graph shows the mean±SD (dotted line) of 3 independent experiments. **e.** Erythromycin induces blebbing, cytoplasmic shrinkage and lysis in *B. vulgatus* and *B. uniformis*. Phase contrast movies of *B. vulgatus* and *B. uniformis* were acquired after ERY treatment (5-fold MIC). Here shown 3 frames of 3 images per strain (time indicated in the upper left corner; t=0 when drug added). White arrows indicate blebs, cytoplasmic shrinkage and bacterial lysis; the scale bar is 5 μm. Movies are available in Supplementary Material (Movies 1-4).
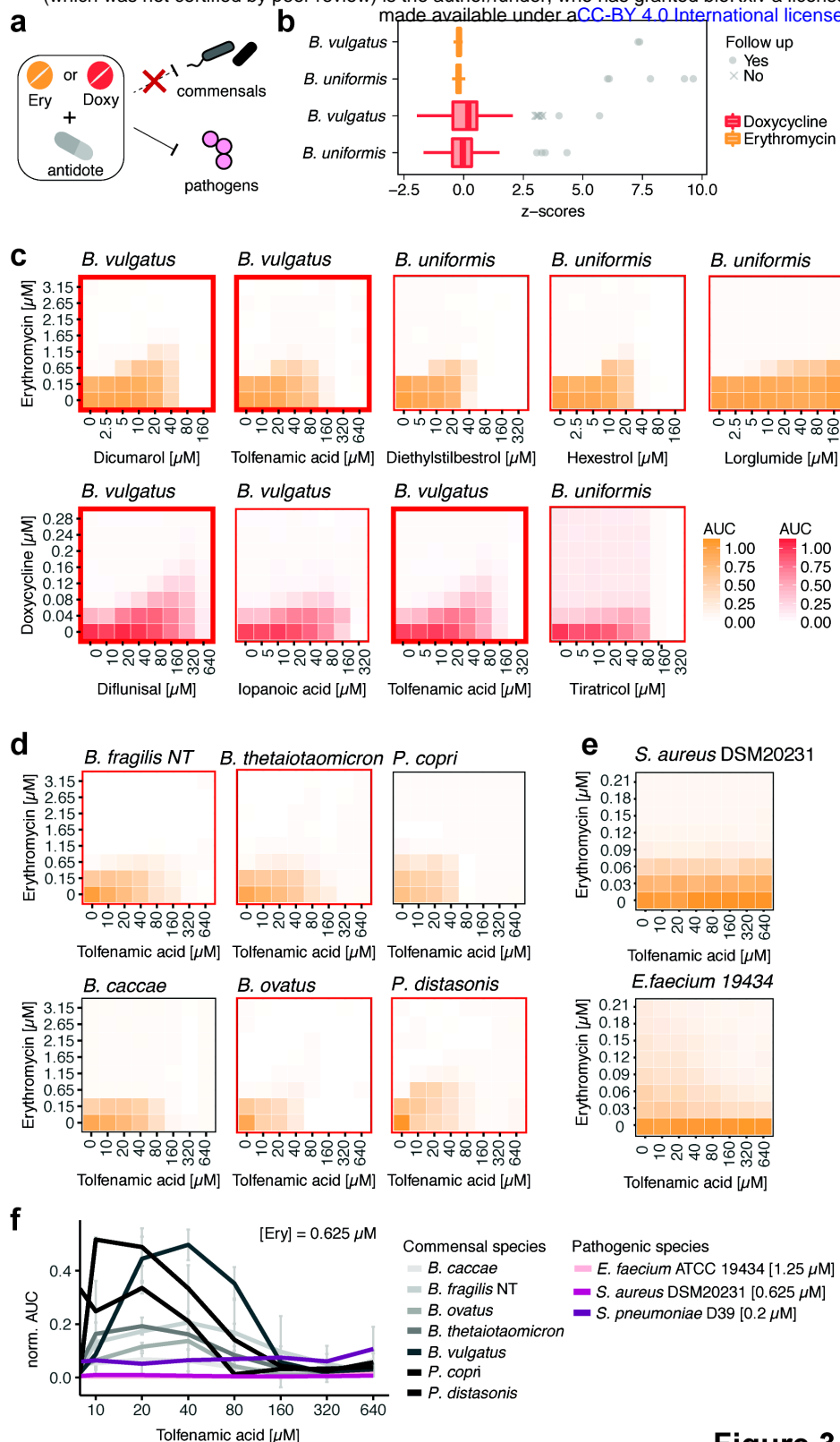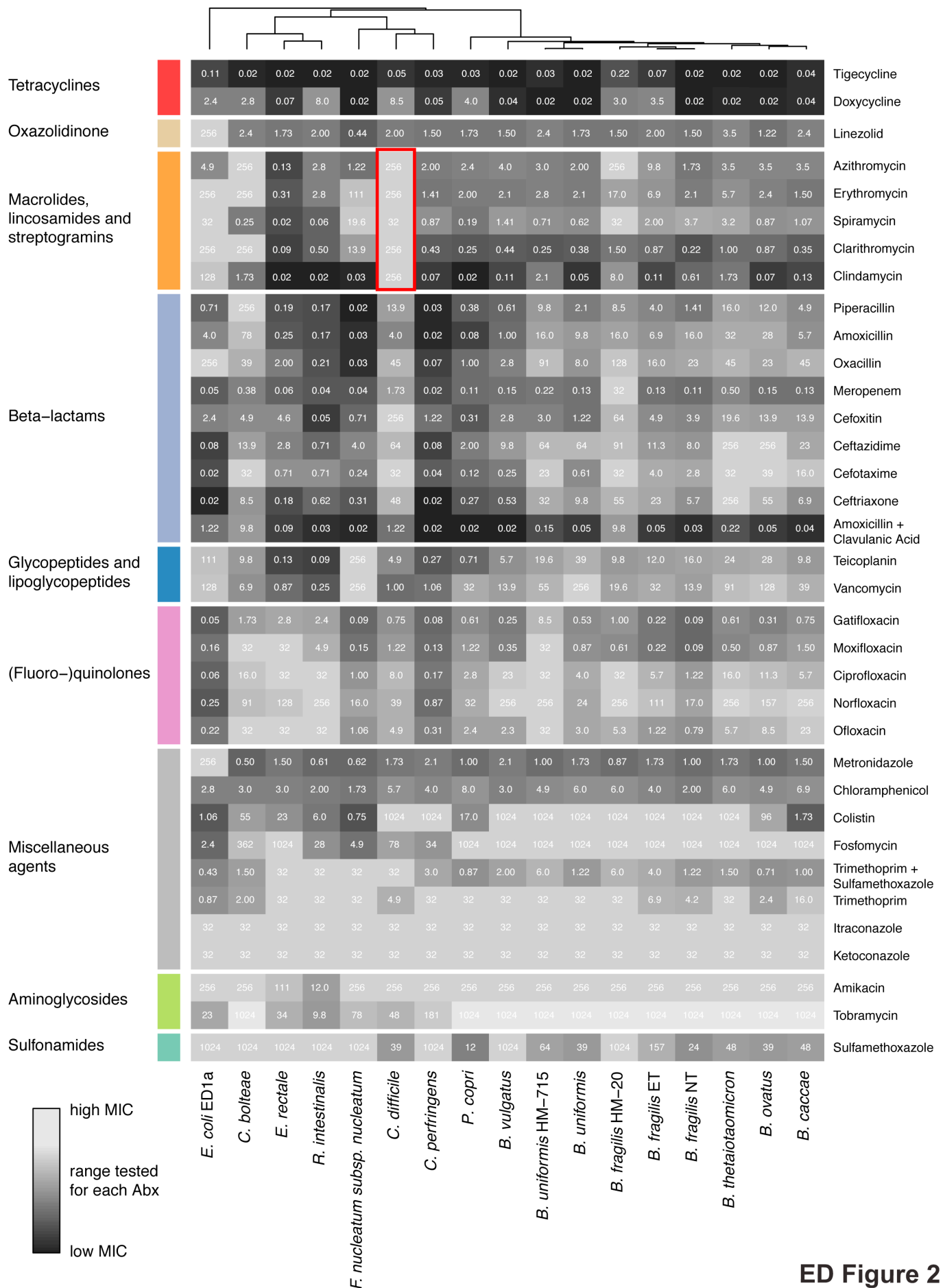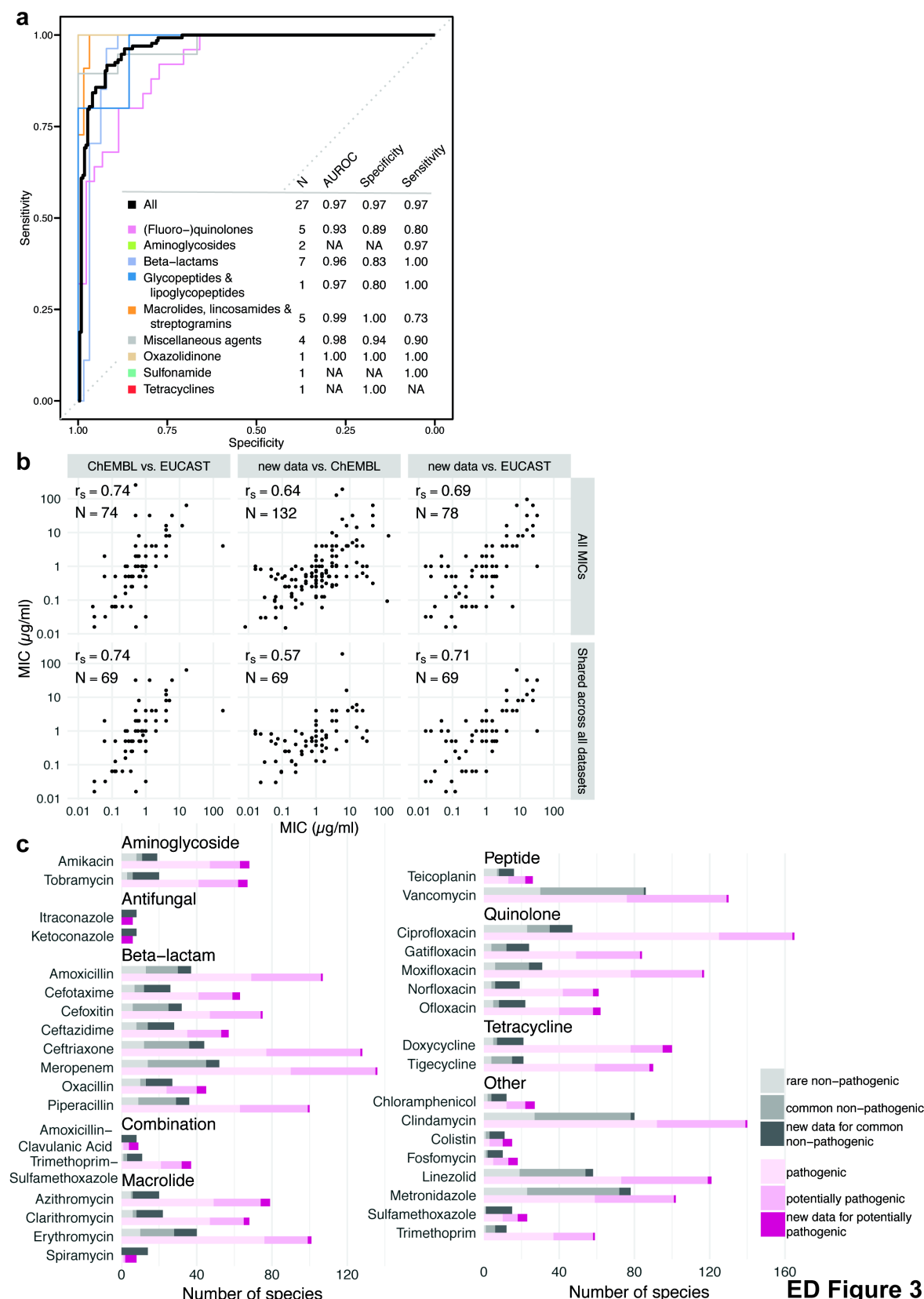
Figure 3

Figure 3 – Antidotes for selective protection of prevalent and abundant gut commensal species from macrolides and tetracyclines.
a. Schematic illustration of the screen concept: searching for antidote compounds that antagonize the antibacterial effect of erythromycin or doxycycline on commensal but not on pathogenic bacteria. **b.** Z-scores on bacterial growth (based on areas under the curve (AUCs)) for combinatorial drug exposure with antibiotic (ERY or DOX) and FDA-approved drug. Compounds that successfully rescued *B. vulgatus* and/or *B. uniformis* growth in the presence of the antibiotic (z-score > 3) are indicated in gray. The strongest hits (circles) were validated further in concentration-dependent assays (Extended Data Fig. 10a). For each antibiotic and each strain, ~1200 drugs were tested in two replicates. Boxplots are defined as in Figure 1d. **c.** For 9 of the validated antagonists, 8 x 8 checkerboard assays were performed to determine concentration ranges of the antagonistic interaction. Heat maps depict bacterial growth based on normalized median of AUCs of 4 replicates. All interactions were antagonistic, and pairs tested further in other commensal species are framed in bold. **d.** Checkerboard assays confirm the ability of tolfenamic acid to protect further gut commensals from growth inhibition by erythromycin. Heat map as in **c**, but for 2 replicates. Antagonistic interactions are framed in red. **e.** Checkerboard of tolfenamic acid with erythromycin reveal neutral interactions in *S. aureus* and *E. faecium* (aerobic conditions). Heat maps as in c, based on at least two independent experiments with two technical replicates each. **f.** Tolfenamic acid concentration-dependent rescue of commensal growth at clinical relevant erythromycin concentrations based on AUCs (anaerobic conditions). Erythromycin still retains its activity against pertinent pathogens such as *S. aureus, E. faecium* and *S. pneumoniae* (aerobic conditions). 0.625 µM correspond to ~0.5 µg/ml erythromycin, which is in the range of the MIC breakpoints for *Staphylococcus* (1 µg/ml), *S. pneumoniae* (0.25 µg/ml) and *Streptococci* groups A, B, C & G (0.25 µg/ml). Error bars depict standard deviation.

ED Figure 1

Extended Data Figure 1 – Effects of 144 antibiotics on 40 human gut commensals
Heat map according to sensitivity or resistance of each strain to the respective antibiotic at a concentration of 20 µM. Antibiotics are grouped according to drug classes and species are clustered according to their responses across the 144 antibiotics tested. Data is replotted from[4]. *Akkermansia muciniphila* (Muc, DSM22959, type strain) is resistant to nearly all quinolone antibiotics (red box). We consolidated this finding by MIC determination for Ciprofloxacin (>32 µg/ml), Gatifloxacin (>32 µg/ml), Moxifloxacin (>32 µg/ml), Norfloxacin (>256 µg/ml) and Ofloxacin (>32 µg/ml).

25

Extended Data Figure 2 – MICs for 17 species on 35 antimicrobials

Heat map depicts MICs for each drug-strain pair in µg/ml. Heat map color gradient is adjusted to the MICs concentration range tested on the respective MIC test strip. Black depicts sensitivity and light grey indicates resistance. Mean values across two biological replicates are shown (Suppl. Table 3). *C. difficile* is particularly resistant to all tested macrolides and clindamycin (red box).

ED Figure 2

26

Extended Data Figure 3 – MIC dataset validates antibiotic sensitivity profiles from the screen dataset and is consistent with publically available MICs.

a. Receiver operating characteristic (ROC) curve analysis was performed to evaluate sensitivity and specificity of the screen[4] using the MIC dataset. Results from the screen were considered as validated if MICs were below/above the 20 μM antibiotic concentration that was tested in the screen (allowing a two-fold error margin). N is the number of antibiotics that we tested both in the screen and determined MICs for, AUROC is the area under the characteristic ROC. TN denotes true negatives, FP false positives, TP true positives, FN false negatives.

b. Comparison including Spearman correlation coefficients of the MICs from this study to MICs from the ChEMBL[27] and EUCAST[24] databases. Panels in the upper row: comparison between all MICs that are shared between the two indicated datasets. Panels in the lower row: comparison of the 69 MICs that are shared across all three datasets. Despite experimental differences, our MICs correlate well with available EUCAST/ ChEMBL data.

c. Number of the sum of new (this study) and already available MICs (EUCAST/ ChEMBL) per drug according to antibiotic class and prevalence/virulence of the bacterial species. The new dataset expands MICs across the board and specifically fills the knowledge gap on non-pathogenic species.
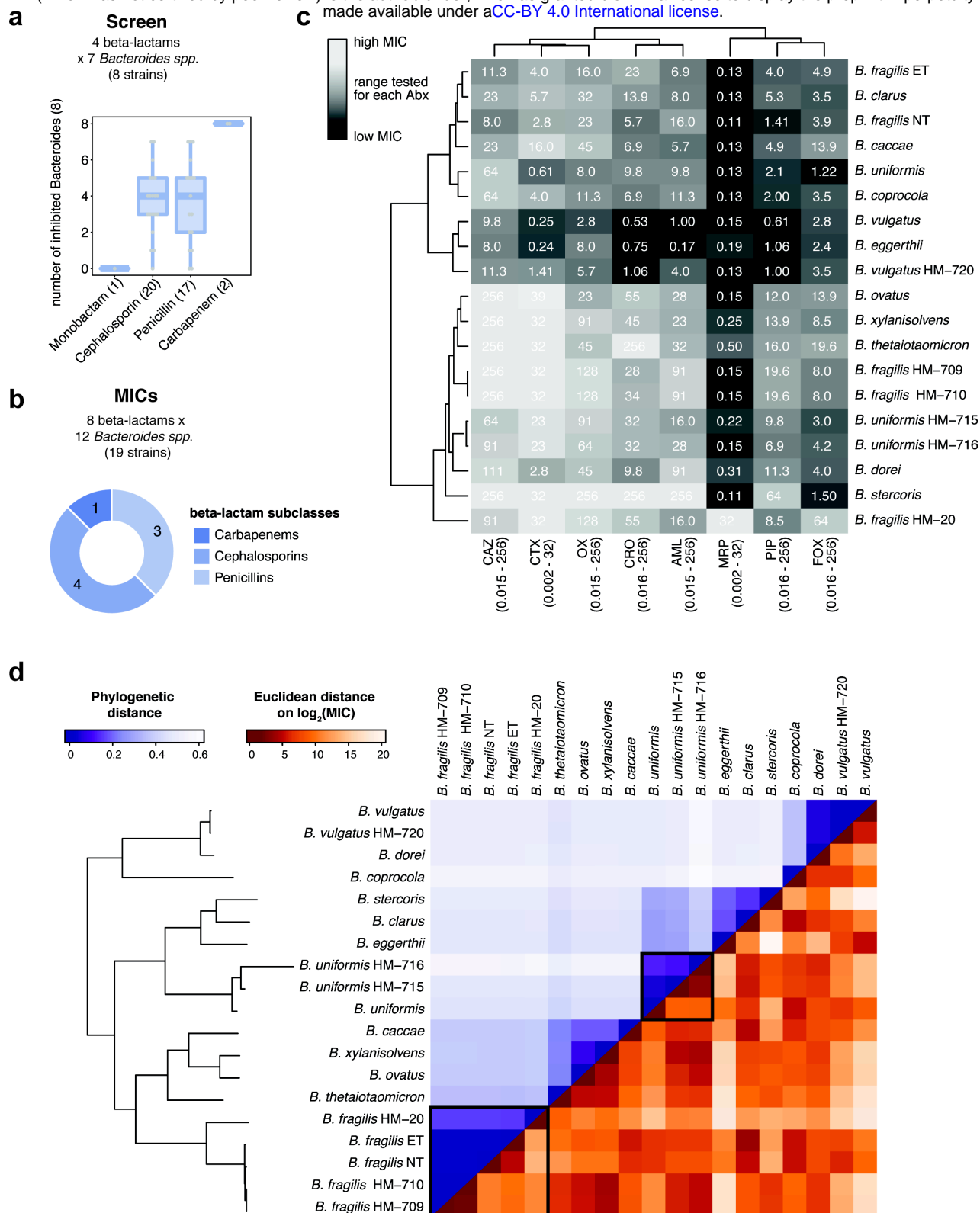
ED Figure 4

Extended Data Figure 4 – β-lactam antibiotic resistance profiles do not recapitulate phylogenetic relationship between *Bacteroides spp.*

a. Number of inhibited *Bacteroides spp.* (out of 8 tested) at 20 μM per β-lactam subclass, based on the initial screen[4]. Number of drugs per class tested are shown in parenthesis. Boxes plotted as in Figure 1d.

b. Overview of the number of drugs tested per β-lactam subclasses on *Bacteroides spp.*; compared to ED Figure 2, 10 additional strains were tested: *B. eggerthii*, *B. clarus*, *B. coprocola*, *B. vulgatus* HM–720, *B. xylanisolvens*, *B. fragilis* HM–709, *B. fragilis* HM–710, *B. uniformis* HM–716, *B. dorei* and *B. stercoris*.

c. MIC heat map for 8 β-lactam antibiotics on 19 *Bacteroides spp.* Strains are clustered according to resistance profiles across all β-lactam antibiotics, drugs are clustered according their effects on *Bacteroides spp.* MICs values are based on two biological replicates and are partially replotted from Extended Data Fig. 2. Heat map gradients are adjusted to the antibiotic concentration ranges tested with lighter color depicting resistance and darker color depicting sensitivity.

d. Heat map of phylogenetic relationship between *Bacteroides spp* (upper triangular matrix) ordered by phylogeny and their resistance profiles across β-lactam antibiotics (lower triangular matrix). Colors represent the pairwise phylogenetic distance and the Euclidean distance on the log2 transformed MICs for β-lactams (panel c). Examples of strains from the same species (*B. fragilis* / *B. uniformis*) that respond differently to β-lactam antibiotics, are highlighted.
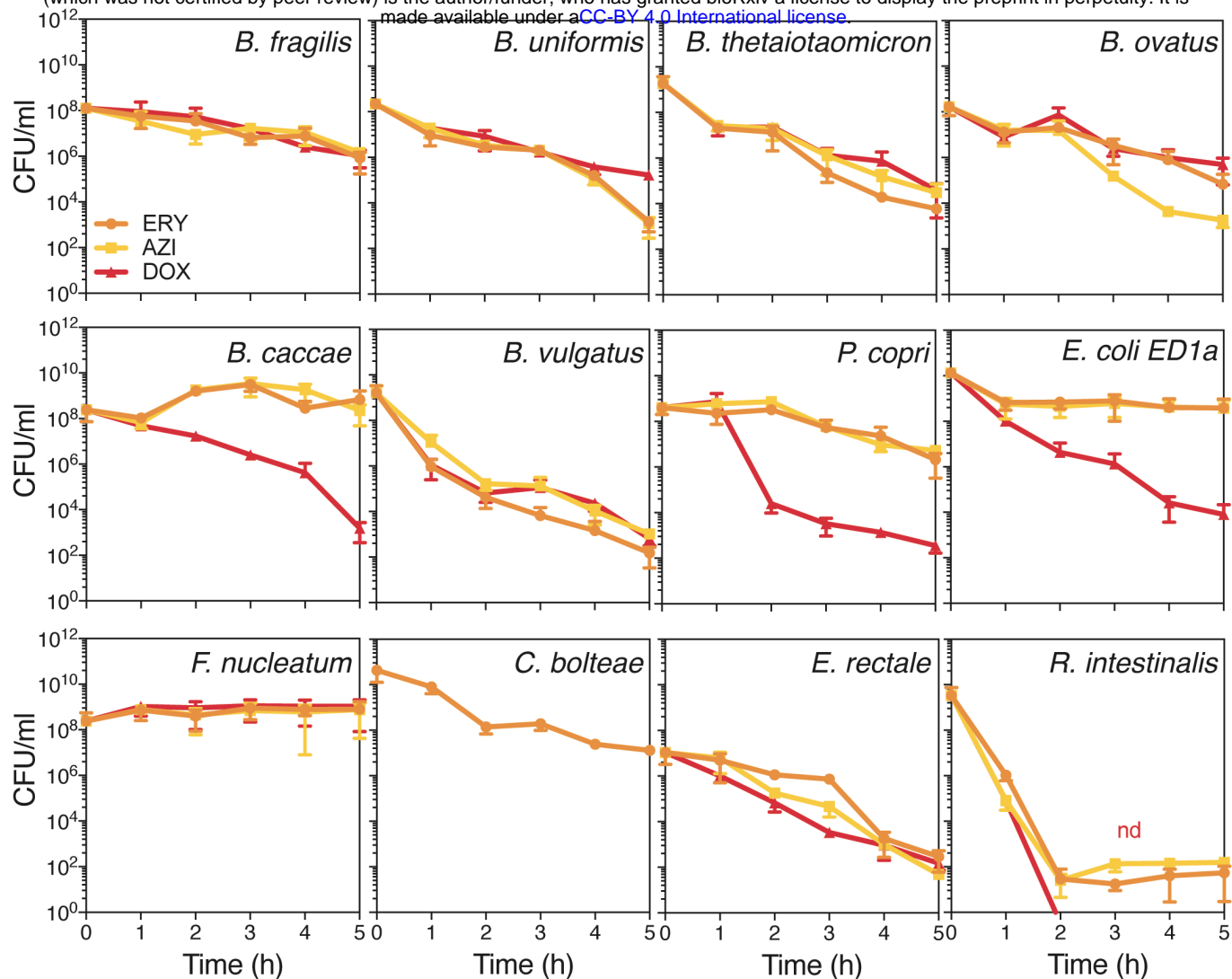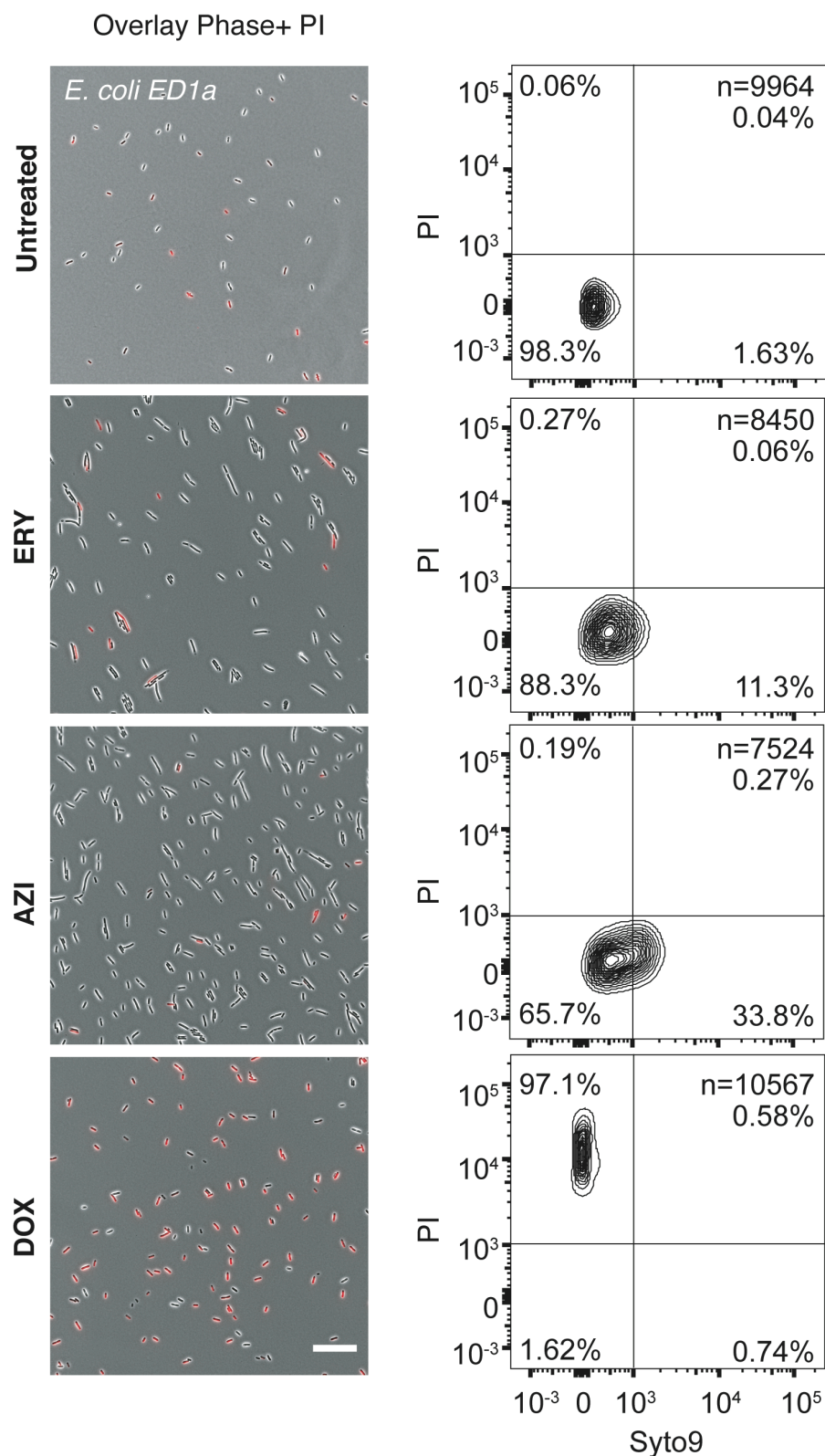
ED Figure 5

Extended Data Figure 5 - Time-kill curves of 12 abundant gut microbes after treatment with macrolides and tetracyclines.
Survival of 12 abundant gut microbes was assessed by CFU counting over a 5 hour-treatment of either ERY, AZI or DOX. This graph shows the mean±SD of 3 independent experiments.

ED Figure 6

Extended Data Figure 6 - Live/dead staining of macrolide or tetracycline-treated *E. coli* ED1a.

The left panel shows an overlay of phase contrast and fluorescence microscopy images of propidium iodide (PI)-stained *E. coli* ED1a before and 5 hours after ERY, AZI or DOX treatments. The number of cells on each frame has no meaning, as cultures were concentrated before imaging; the scale bar is 10 μM. The right panel shows the corresponding quantification of live/dead-stained cells by flow cytometry with Syto9 on the x-axis (live cells) and PI on the y-axis (dead cells). Both the total number of measured events (n) and the percentage of cells found in each quadrant are indicated on the graphs.
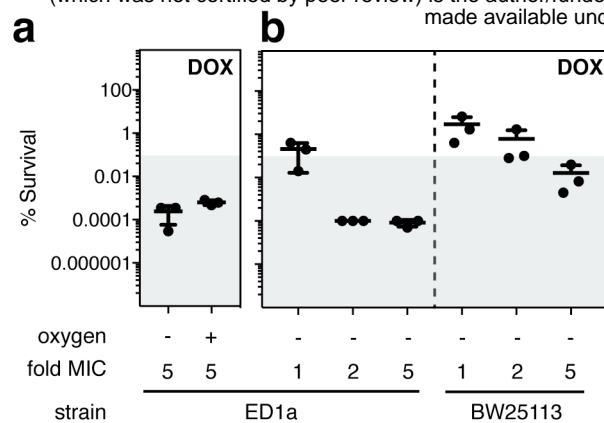
ED Figure 7

Extended Data Figure 7 - Effect of oxygen and strain specificity on survival after doxycycline treatment
a. The survival of *E. coli* ED1a was assessed after a 5-hour treatment with 5-fold MIC of DOX in the presence or absence of oxygen. Killing was similarly effective in both conditions.
b. The survival of *E. coli* ED1a and *E. coli* BW25113 were assessed after a 5-hour treatment with 1, 2 and 5-fold MIC of DOX in MGAM medium in anaerobic conditions. The lab strain is more resistant to killing with doxycycline becoming boarder-line bactericidal at higher MICs.
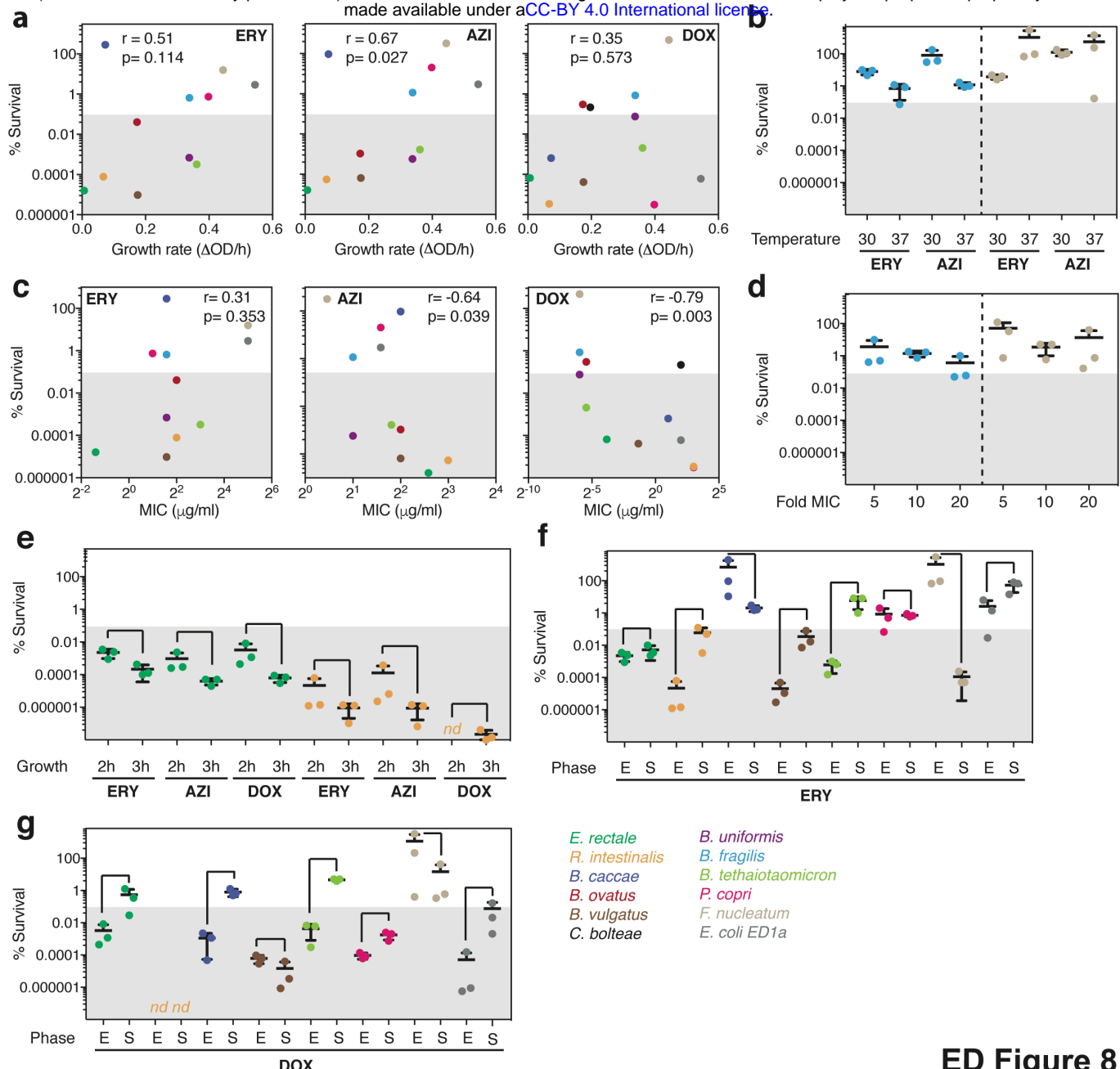
ED Figure 8

Extended Data Figure 8 – Assessing potential confounding factors for the killing capacities of erythromycin, azithromycin and doxycycline

a. Scatter plot of individual bacterial growth rates and percentage survival after a 5-hour treatment with 5-fold MIC of ERY, AZI or DOX treatments. *r* indicates the Spearman correlation coefficient. Tested species are color-coded here and in all panel thereafter as indicated in the bottom of this figure. Positive correlations for macrolides were tested further in **b** to check if changing growth rate in same species affects percentage killed.

b. The survival of *B. fragilis* (blue) and *F. nucleatum* (beige) were assessed after a 5-hour macrolide treatment (5-fold MIC of ERY and AZI) at either 30°C (slow growth) or 37°C (fast growth) to test the effect of slowing down growth on survival. No significant change observed. This graph shows the mean±SD of three independent experiments.

c. Scatter plot of MICs and percentage survival after a 5-hour treatment with 5-fold MIC of ERY, AZI or DOX treatments. *r* indicates the Spearman correlation coefficient. Doxycycline exhibited a strong and significant anti-correlation, that is that species which were more sensitive to doxycycline (lower MIC) were not killed when they were treated with 5-fold MIC concentrations. Thus, we tested further whether increasing the drug concentration in some of those sensitive strains decreased the % of survival (panel **d**).

d. The survival of *B. fragilis* (blue) and *F. nucleatum* (beige) were assessed after a 5-hour treatment with increasing concentrations of DOX (5, 10 or 20- fold of MIC) to test whether higher concentrations of DOX induced more killing. This seemed not be the case. This graph shows the mean±SD of three independent experiments.

e. To evaluate whether outgrowth of stationary phase and homogeneity of population affected our results, we selected two slow-growing strains, *E. rectale* and *R. intestinalis* and grew for 2 or 3 hours after being diluted from an overnight culture to an OD$_{578}$ 0.01. Both strains were then treated for 5 hours with 5-fold MIC of ERY, AZI or DOX and their survival was assessed to test the impact of the growth phase on the percentage survival. Although slight differences were observed and 3h grown cultures were killed more effectively (presumably because more cells had exited stationary phase and were growing exponentially by then), the general trends remained the same. If anything, this means that we are underestimating the killing for slow-growers, since we performed all other experiments with 2 hours outgrowth. This graph shows the mean±SD of three independent experiments.

f. The survival of 8 selected gut microbes was measured after treating cells in exponential phase (E – 2 hours after dilution from an overnight culture) or in stationary phase (S – overnight growth) with 5-fold MIC of ERY for 5 hours to test the impact of the growth phase on the percentage survival. As expected, survival is higher in stationary phase for half of the strains, but in some cases stationary phase cells were as or more sensitive than exponentially growing cells – this is the case for *B. caccae* and *F. nucleatum*. This graph shows the mean±SD of three independent experiments.

g. Same as in **f** but with DOX. Similar effects observed as in f, with more than half of strains becoming more resistant in stationary phase.

32
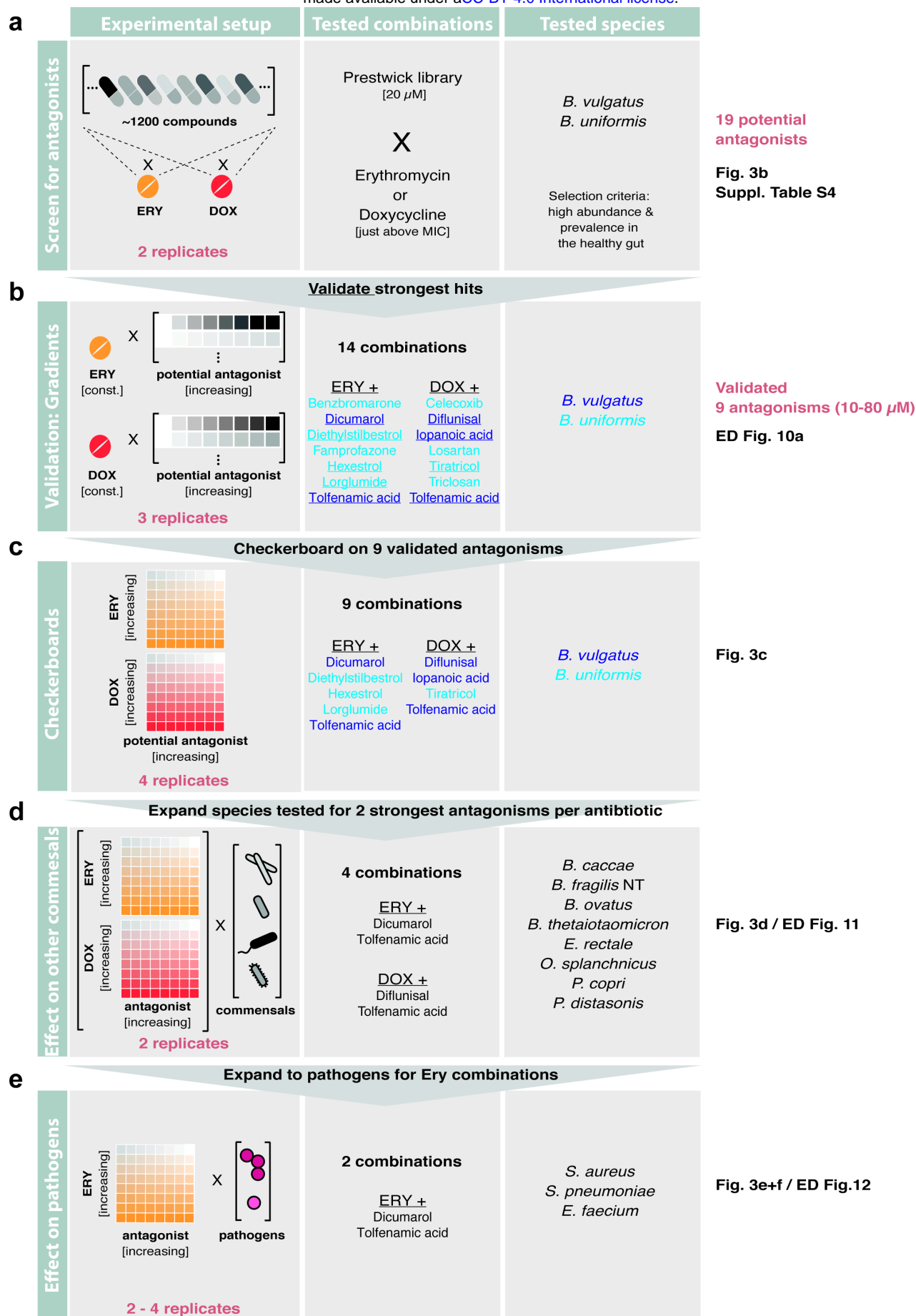
Extended Data Figure 9 – Schematic overview of screen for microbiome-protective antibiotic antagonisms
Workflow with decision process on which antagonist to move on to next evaluation step.
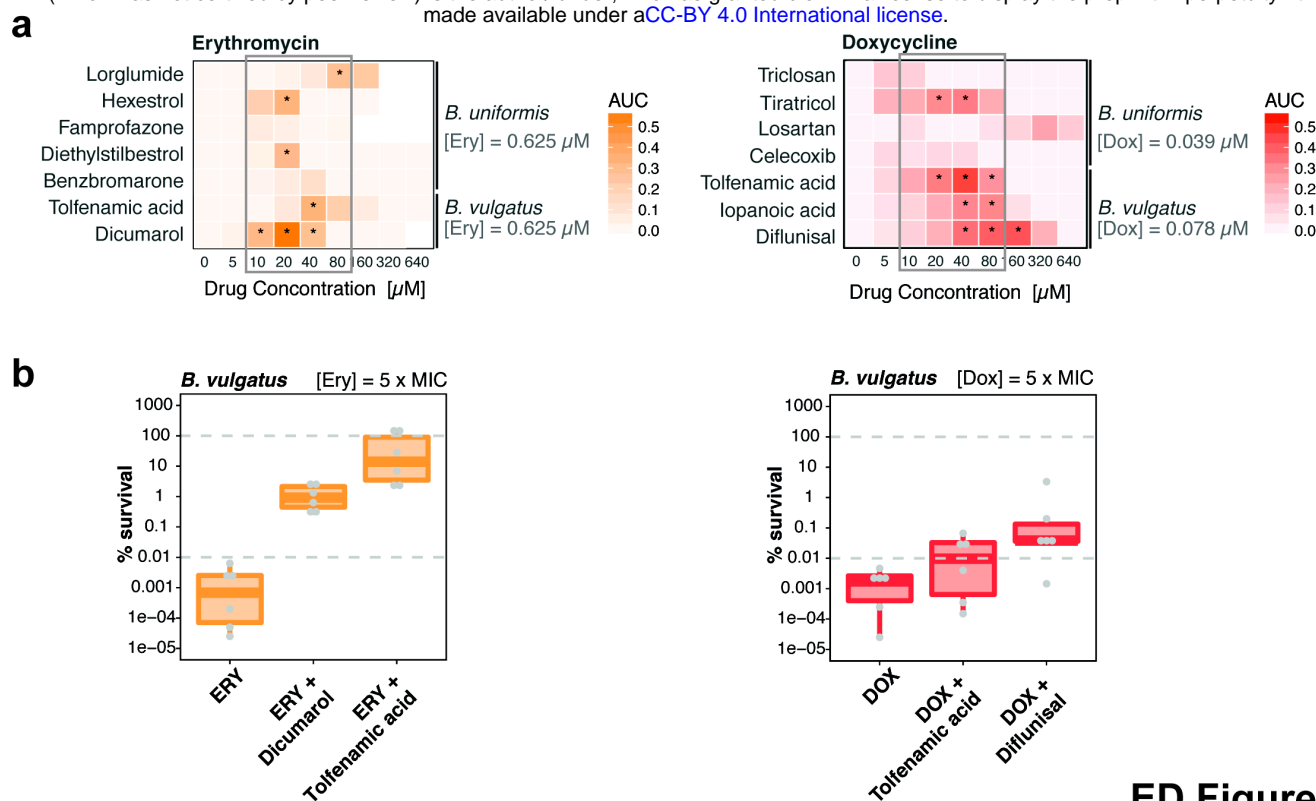
ED Figure 10

Extended Data Figure 10 – Validation of potential microbiome-protective antagonists

a. Validation of the strongest antagonists in independent experiments. Erythromycin and doxycycline concentrations were kept constant ([ERY]=0.625 µM, [DOX] = 0.039 / 0.078 µM) and concentration ranges were tested for antagonist. Asterisks indicate that at least 25% of the bacterial growth (compared to no drug controls) could be rescued by the antagonist at a given concentration. Heat map depicts median AUCs across triplicates.

b. Percentage of surviving *B. vulgatus* cells were determined after 5 h incubation with either erythromycin (3.25µM) or doxycycline (0.4 µM) alone or in presence of the antagonist dicumarol (20 µM), tolfenamic acid (40 µM) or diflunisal (80 µM). Data is based on 3 independent experiments. Boxplots are plotted as in Figure 1d.
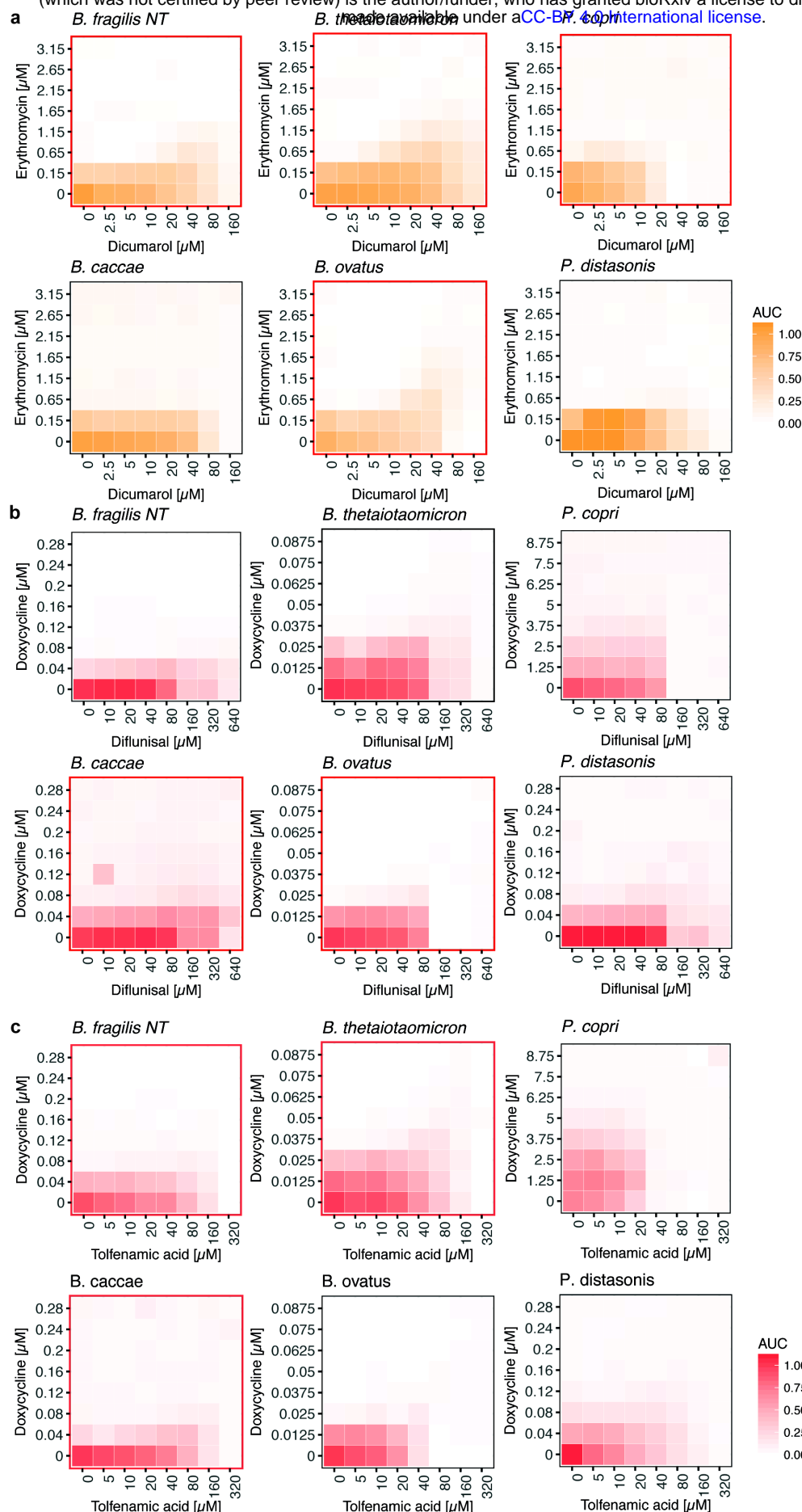
ED Figure 11

Extended Data Figure 11 – Effect of antidotes on further gut commensals

8 x 8 checkerboard assays to investigate if antidote is also protective for additional gut commensals for the following combinations: erythromycin and dicumarol (**a**), doxycycline and diflunisal (**b**) and doxycycline and tolfenamic acid (**c**). Heat map depicts bacterial growth based on median AUCs from two independent replicates. Red contours indicate antagonistic drug interactions.
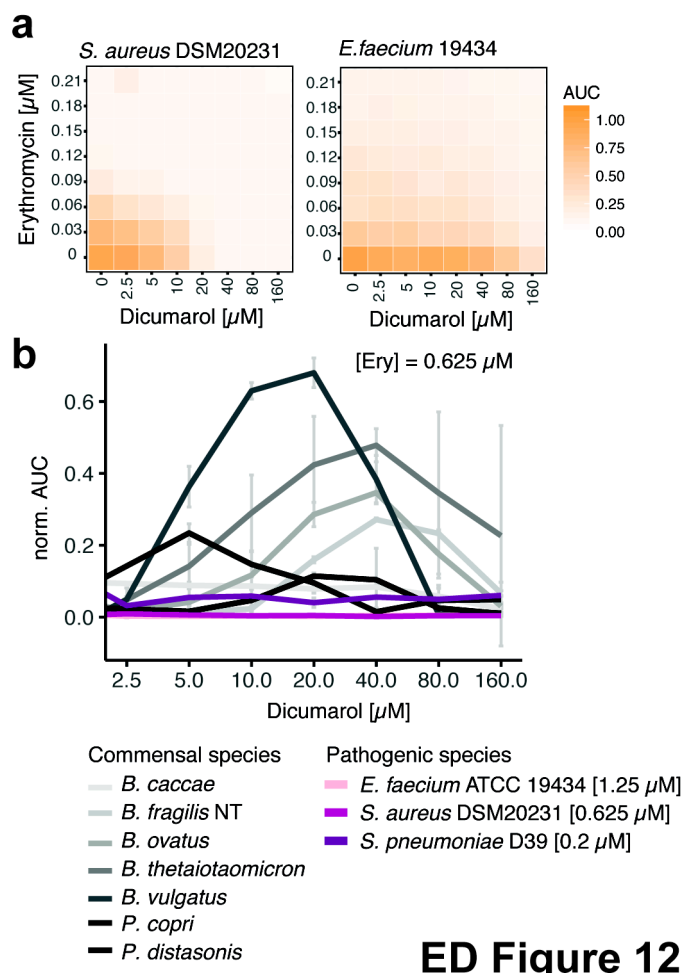
ED Figure 12

Extended Data Figure 12– Effect of the antidote dicumarol on pathogens, relatively to commensal species.
a. Checkerboard assays for the drug combinations erythromycin-tolfenamic acid and erythromycin-dicumarol on the pathogens *S. aureus* (two different strains) and *E. faecium*. Heat map depict median normalized AUCs of checkerboard assays (at least three independent replicates).
b. Dicumarol rescues commensal growth (based on median AUCs, N=2) at clinical relevant erythromycin concentrations in a concentration-dependent manner. Erythromycin still retains its activity against pertinent pathogens such as *S. aureus*, *E. faecium* and *S. pneumoniae* and is even slightly more active (synergy) for *E. faecium* (based on median AUCs, N=3). Error bars depict standard deviation.